Energy, Mines and Resources Canada

Énergie, Mines et Ressources Canada

CANMET

Canada Centre for Mineral and Energy Technology

Centre canadien de la technologie des minéraux et de l'énergie

Mining Research Laboratories

Laboratoires de recherche minière

Canada

HIGH TEMPERATURE UNIAXIAL COMPRESSION TESTS ON URL ROCK SAMPLES FROM BOREHOLES 209-021-SV1 AND 209-030-DIL1

J.S.O. Lau and B. Gorski September 1989

Mining Research Laboratories
Divisional Report MRL 89-90(TR)

This document is an unedited report prepared primarily for discussion and information purposes. It does not necessarily represent final expression of the opinion of the Canada Centre for Mineral and Energy Technology (CANMET)

Le présent document est un rapport préliminaire rédigé principalement en vue de discussion et de renseignements généraux. Il ne représente nullement l'expression définitive de l'opinion du Centre canadien de la technologie des minéraux et de l'énergie (CANMET)

72 pp

MICROMEDIA

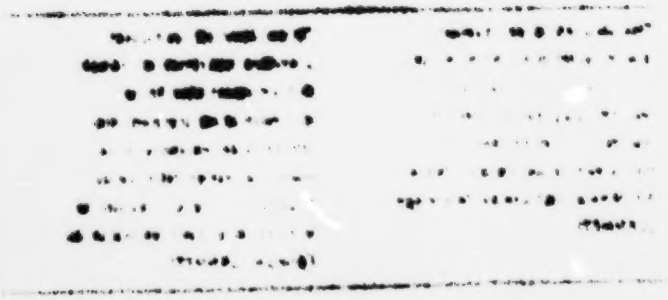

90-01327/

HIGH TEMPERATURE UNIAXIAL COMPRESSION TESTS ON URL ROCK SAMPLES FROM BOREHOLES 209-021-SV1 AND 209-030-DIL1

by

J.S.O. Lau[1] and B. Gorski[2]

ABSTRACT

A series of ambient and high temperature uniaxial compression tests were conducted on grey granitic core samples obtained from Boreholes 209-021-SV1 and 209-030-DIL1 located at the 240 level of Atomic Energy of Canada Limited's Underground Research Laboratory (URL). Three sets of tests at three temperatures (25°, 75° and 125° C) were conducted to obtain high temperature uniaxial compressive strength data, and to study the behaviour of rock specimens at high temperature under unconfined conditions.

The mean uniaxial compressive strength was found to decrease by approximately 6 MPa when the temperature was raised from 75° to 125° C. Temperature had little effect on the tangent Young's modulus and pseudo Young's modulus. Poisson's ratio decreased only when the temperature increased from 25° to 75° C. Temperature had no effect on the angle of internal friction and the cohesive strength.

The effect of temperature on the predicted uniaxial compressive strength of the intact rock material, σ_c, and the material constant m derived from the Hoek and Brown failure criterion is not clear. The value of σ_c appeared to decrease when the temperature was raised from 75° to 125° C.

Rock specimens from Borehole 209-021-SV1 were found to be stronger and stiffer than those from Borehole 209-030-DIL1.

---

[1]Geotechnical Engineer, Atomic Energy of Canada Limited, on attachment to Canadian Mine Technology Laboratory, Mining Research Laboratories, CANMET, Energy, Mines and Resources Canada, Ottawa, Ontario.

[2]Rock Mechanics and Development Technologist, Canadian Mine Technology Laboratory, Mining Research Laboratories, CANMET, Energy, Mines and Resources Canada, Ottawa, Ontario.

Keywords: uniaxial, compression, high temperature, strength, elastic, dynamic, strain, Young's modulus, Poisson's ratio, failure criterion

ESSAIS DE COMPRESSION UNIAXIALE HAUTE TEMPÉRATURE SUR DES CAROTTES PROVENANT DES TROUS DE SONDE 209-021-SV1 ET 209-030-DIL1 DU LRS

par

J.S.O. Lau[1] et B. Gorski[2]

RÉSUMÉ

Une série d'essais de compression uniaxiale à la température ambiante et haute température ont été réalisés sur des carottes de granite gris prélevées dans les trous de sonde 209-021-SV1 et 209-030-DIL1 forés au niveau 240 du Laboratoire de recherche souterrain de L'Énergie atomique du Canada Limitée. Trois séries d'essais ont été menés à trois températures différentes (25°, 75° et 125° C) afin d'obtenir des données sur la résistance à la compression uniaxiale à haute température et pour analyser le comportement d'échantillons à haute température dan des conditions non confinées.

La résistance à la compression uniaxiale moyenne a diminué d'environ 6 MPa lorsque la température est passée de 75° à 125° C. La température a eu peu d'effets sur le module de Young tangent et le pseudo module de Young. Le coefficient de Poisson n'a diminué que lorsque la température est passée de 25° à 75° C. La température n'a eu aucun effet sur l'angle de frottement interne et la résistance due à la cohésion.

L'effet de la température sur la résistance à la compression uniaxiale prévue de la roche intacte, σ_c, et la constante du matériau m dérivée du critère de rupture de Hoek et Brown ne ressort pas clairement. La valeur de σ_c semble n'avoir diminué que lorsque la température a été augmentée de 75° á 125° C.

Les échantillons de roche provenant du trou de sonde 209-021-SV1 se sont révélés plus résistants et plus durs que ceux provenant du trou de sonde 209-030-DIL1.

---

[1]Ingénieur géotechnique, L'Énergie atomique de Canada Limitée, détaché au Laboratoire canadien de la technologie minière, Laboratories de recherche minière, CANMET, Énergie, Mines et Ressources Canada, Ottawa, Ontario.

[2]Spécialiste en mécanique des roches et technique de développement, Laboratoire canadien de la technologie minière, Laboratoires de recherche minière, CANMET, Énergie, Mines et Ressources Canada, Ottawa, Ontario.

Temes-clés: compression uniaxiale, haute température, résistance, déformation, module de Young, élastique, dynamique, coefficient de Poisson, critère de rupture.

TABLE OF CONTENTS

	Page No.
Abstract	i
Résumé	ii
Table of contents	iii
List of tables	iv
List of figures	v
1. Introduction	1
2. Sampling and specimen preparation	2
3. Dynamic elastic properties	2
4. Test apparatus and procedure	4
5. Uniaxial testing program	5
6. Results and discussion	5
6.1 Test results	5
6.2 Effect of temperature on uniaxial compressive strength	6
6.3 Effect of temperature on axial strain at failure	7
6.4 Effect of temperature on tangent Young's modulus	7
6.5 Effect of temperature on pseudo Young's modulus	8
6.6 Effect of temperature on Poisson's ratio	9
6.7 Effect of temperature on strength properties	9
7. Conclusions	12
8. Recommendations	13
Acknowledgements	13
References	14
Appendix A	50
Appendix B	60

LIST OF TABLES

Table		Page No.
1.	Dimensions, densities and dynamic elastic properties of rock samples from Borehole 209-021-SV1	16
2.	Dimensions, densities and dynamic elastic properties of rock samples from Borehole 209-030-DIL1	17
3.	Results of ambient temperature and high temperature uniaxial tests on rock samples from Borehole 209-021-SV1	18
4.	Results of ambient temperature and high temperature uniaxial tests on rock samples from Borehole 209-030-DIL1	19
5.	Tangent Young's moduli of rock samples from Borehole 209-021-SV1	20
6.	Tangent Young's moduli of rock samples from Borehole 209-030-DIL1	21
7.	Pseudo Young's moduli of rock samples from Borehole 209-021-SV1	22
8.	Pseudo Young's moduli of rock samples from Borehole 209-030-DIL1	23
9.	Values of σ_c, m, s and r^2 obtained from Borehole 209-021-SV1	24
10.	Values of σ_c, m, s and r^2 obtained from Borehole 209-030-DIL1	25
11.	Results of Mohr's circle analysis for Borehole 209-021-SV1	26
12.	Results of Mohr's circle analysis for Borehole 209-030-DIL1	27

LIST OF FIGURES

Figure		Page No.
1.	Plot of uniaxial compressive strength versus temperature for Borehole 209-021-SV1	28
2.	Plot of uniaxial compressive strength versus temperature for Borehole 209-030-DIL1	29
3.	Plots of tangent Young's modulus versus normalized axial stress for Borehole 209-021-SV1	30
4.	Plots of tangent Young's modulus versus normalized axial stress for Borehole 209-030-DIL1	31
5.	Plot of tangent Young's modulus versus temperature for Borehole 209-021-SV1	32
6.	Plot of tangent Young's modulus versus temperature for Borehole 209-030-DIL1	33
7.	Plots of pseudo Young's modulus versus normalized axial stress for Borehole 209-021-SV1	34
8.	Plots of pseudo Young's modulus versus normalized axial stress for Borehole 209-030-DIL1	35
9.	Plot of pseudo Young's modulus versus temperature for Borehole 209-021-SV1	36
10.	Plot of pseudo Young's modulus versus temperature for Borehole 209-030-DIL1	37
11.	Plot of Poisson's ratio versus temperature for Borehole 209-021-SV1	38
12.	Plot of Poisson's ratio versus temperature for Borehole 209-030-DIL1	39
13.	Hoek and Brown failure envelope for samples from Borehole 209-021-SV1 tested at 25° C	40
14.	Hoek and Brown failure envelope for samples from Borehole 209-021-SV1 tested at 75° C	41
15.	Hoek and Brown failure envelope for samples from Borehole 209-021-SV1 tested at 125° C	42
16.	Hoek and Brown failure envelope for samples from Borehole 209-030-DIL1 tested at 75° C	43
17.	Hoek and Brown failure envelope for samples from Borehole 209-030-DIL1 tested at 125° C	44

18. Mohr circles and failure envelope for samples from Borehole 209-021-SV1 tested at 25° C 45
19. Mohr circles and failure envelope for samples from Borehole 209-021-SV1 tested at 75° C 46
20. Mohr circles and failure envelope for samples from Borehole 209-021-SV1 tested at 125° C 47
21. Mohr circles and failure envelope for samples from Borehole 209-030-DIL1 tested at 75° C 48
22. Mohr circles and failure envelope for samples from Borehole 209-030-DIL1 tested at 125° C 49

1. Introduction

A joint research project has been undertaken by the Canada Centre for Mineral and Energy Technology (CANMET) and Atomic Energy of Canada Limited (AECL) to gain an understanding of the stability and deformability at high temperature of the rock mass at AECL's Underground Research Laboratory (URL) located near Lac du Bonnet, Manitoba. Geotechnical research carried out at URL constitutes a major component of the Canadian Nuclear Fuel Waste Management Program (Simmons and Soonawala, 1982) concerned with the safe, long term disposal of high level nuclear wastes in vaults located at depth in a pluton.

Several series of high temperature triaxial tests have been carried out on rock core samples from boreholes drilled in the URL and from surface boreholes drilled at the site of the URL to investigate the thermo-mechanical properties of the rock mass. These tests were conducted at confining pressure levels ranging from 3.5 to 35.0 MPa. The test results have been described in detail by Annor et al. (1981), Jackson (1984), Annor and Jackson (1985), Annor and Jackson (1987), Lau et al. (1988a) and Lau et al. (1988b). They reported that the triaxial compressive strengths of the core samples increased with increasing confining pressure and decreased with increasing temperature. The greatest decrease occurred at the low confining pressure of 3.5 MPa. At higher confining pressure levels, the effect of temperature on the strength of the samples became less significant. Temperature was found to have no effect on the deformability of the samples at confining pressure levels above 3.5 MPa. At the low confining pressure of 3.5 MPa, the 50% tangent Young's modulus decreased with increasing temperature.

Lau et al. (1988a) and Lau et al. (1988b) also suggested that the value of the material constant m in the Hoek and Brown failure criterion (Hoek and Brown, 1980) increased, but the predicted uniaxial compressive strength of the intact rock material, σ_c, decreased with increasing temperature. However, the absence of the laboratory high temperature uniaxial compressive strength and tensile strength data created some uncertainties in the computation of those values. A program was initiated late in 1988 to perform high temperature uniaxial compression tests on URL rock samples to obtain high temperature uniaxial compressive strength data in the laboratory. It was felt that the test results would not only eliminate some of the uncertainties but also give a better insight into the behaviour of the rock samples at high temperature under unconfined conditions.

This report presents the results of the uniaxial compression testing program conducted at temperatures of 25°, 75° and 125° C on rock samples obtained from Boreholes 209-021-SV1 and 209-030-DIL1 drilled at the 240 Level in the URL.

2. Sampling and specimen preparation

Samples used in these tests were NQ rock cores obtained from Borehole 209-021-SV1 between the downhole lengths of 4.05 and 5.46 m and from Borehole 209-030-DIL1 between 2.38 and 3.86 m. The rock is a massive, grey, medium to coarse grained granite, composed of quartz, K-feldspar, plagioclase and biotite.

Specimens with ends ground parallel to within 0.025 mm were prepared from the samples in accordance to the procedure described in the Pit Slope Manual Supplement 3-5 (Gyenge and Ladanyi, 1977) and the method suggested by the International Society for Rock Mechanics (Brown, 1981).

The dimensions and bulk densities of the specimens are shown in Tables 1 and 2. The lengths and diameters of the specimens varied from 104.44 to 112.83 mm and from 44.88 to 45.23 mm respectively, with length to diameter ratios ranging from 2.3 to 2.5.

The seven specimens to be tested at room temperature were gauged. Micro-measurements type EA-06-500BH-120 gauges with a gauge factor of 2.04 were used. Two diametrically opposite axial strain gauges were mounted at the mid-height of each of the specimens and two circumferential strain gauges were similarly mounted at 90° to the axial gauges. In both cases, the two strain gauges were connected in series to form a single active gauge.

3. Dynamic elastic properties

Prior to high temperature uniaxial compression testing, compression and shear wave velocity measurements were made on the specimens to determine their dynamic elastic constants. The velocity measurements were made in accordance with the procedures described in the Instruction Manual - Sonic Velocity Equipment (Terrametric, 1980) and the Pit Slope Manual Supplement 3-2 (Gyenge and Herget, 1977). The compression and shear wave velocities were determined from compression and shear wave transit times made along the cylindrical axes of the specimens. The dynamic elastic constants were computed from them using the following equations:

Dynamic Young' modulus of elasticity:

$$E_u = \frac{\rho V_s^2 (3V_p^2 - 4V_s^2)}{V_p^2 - V_s^2} \qquad (1)$$

where E_u = dynamic Young's modulus of elasticity
V_p = compression wave velocity
V_s = shear wave velocity
ρ = bulk density

Dynamic shear modulus:

$$G_u = \rho V_s^2 \tag{2}$$

where G_u = dynamic shear modulus

Dynamic Poisson's ratio:

$$\nu_u = \frac{V_p^2 - 2V_s^2}{2(V_p^2 - V_s^2)} \tag{3}$$

where ν_u = dynamic Poisson's ratio

The compression wave velocity, shear wave velocity, dynamic Young's modulus, dynamic shear modulus and dynamic Poisson's ratio determined for each of the specimens are shown in Tables 1 and 2.

Rock samples from Borehole 209-021-SV1 had compression wave velocities ranged from 4.711 to 5.515 km/s with a mean value of 5.030 km/s and a standard deviation (s.d.) of 0.270 km/s; shear wave velocities ranged from 2.732 to 2.949 km/s and had a mean value of 2.832 km/s (s.d. = 0.078 km/s); dynamic Young's moduli ranged from 48.93 to 57.70 GPa with a mean value of 53.39 GPa (s.d. = 3.07 GPa); dynamic shear moduli ranged from 19.62 to 22.88 GPa with a mean value of 21.11 GPa (s.d. = 1.16 GPa); and dynamic Poisson's ratios ranged from 0.24 to 0.32 with a mean value of 0.26 (s.d. = 0.03).

The compression wave velocities of the rock samples from Borehole 209-030-DIL1 were found to range from 4.448 to 4.828 km/s with a mean value of 4.631 km/s (s.d. = 0.128 km/s). Shear wave velocities ranged from 2.615 to 2.775 km/s with a mean value of 2.703 km/s (s.d. = 0.062 km/s). Dynamic Young's moduli ranged from 44.46 to 50.03 GPa with a mean value of 47.76 GPa (s.d. = 2.21 GPa) and dynamic shear moduli ranged from 17.99 to 20.18 GPa with a mean value of 19.24 GPa (s.d = 0.87

GPa). Dynamic Poisson's ratios ranged from 0.23 to 0.26 with a mean value of 0.24 (s.d. = 0.01).

Compression wave velocities, shear wave velocities, dynamic Young's moduli and dynamic shear moduli for rock specimens from Borehole 209-021-SV1 were found to be higher than those for specimens from Borehole 209-030-DIL1.

4. Test apparatus and procedure

The apparatus used to carry out the uniaxial compression tests was a MTS 815 Rock Mechanics Test System. The MTS system is a servo-hydraulic press consisting of a 2.22 MN rated load cell, load frame, hydraulic power supply, triaxial cell, test controller, test processor, temperature controller and DEC micro PDP 11/73 computer. The triaxial cell is rated up to 200° C and equipped with a heater, heat shroud, thermocouples, three linear variable differential transducers (LVDTs) for the measurement of axial strain and an extensometer with a circumferential kit for the measurement of circumferential strain. For a detailed description of the MTS system and its operation, the reader is referred to the MTS Operation Manual (MTS Systems Corp., 1986) and CANMET Division Report MRL 87-33(INT) (Gorski, 1987).

The procedure used to carry out the uniaxial tests at room temperature conformed with the uniaxial compression test procedure described in the Pit Slope Manual Supplement 3-2 (Gyenge and Herget, 1977). The axial and circumferential strain gauges were connected through a B & K type 1526 strain indicator in a half-bridge configuration to the test processor in the MTS system for the measurement of axial and circumferential strains.

The procedure used to conduct the uniaxial tests at high temperature was similar to the high temperature triaxial test procedure outlined in CANMET Division Report MRL 88-90(TR) (Lau et al., 1988a). Instrumented rock specimens (LVDTs, extensometer and heater) were placed in the triaxial cell which was then filled with Syltherm 800 heat transfer fluid. No confining pressure was applied to simulate the uniaxial testing condition. The hydrostatic pressure under this condition was very low (less than 3 kPa) and considered negligible. The confining fluid was then heated at a rate of 1° C per minute until the test temperature was reached. A soak time of one hour was allowed to ensure even heat distribution throughout the specimen before testing.

All specimens were loaded at a constant rate of 1 kN per second under computer control. Signals from the load cell, LVDTs, extensometer and strain gauges were scanned

by the computer every second. The signals were converted to engineering units and measurements from the LVDTs were corrected for end platen compression. The data were stored on hard disk in the micro PDP 11/73 computer and later transferred to the VAX computer for data analysis and plotting.

5. Uniaxial testing program

Testing took place at Canadian Mine Technology Laboratory, Mining Research Laboratories, CANMET, Energy, Mines and Resources Canada in Ottawa in August, 1989. Initially, the uniaxial testing program consisted of three sets of tests conducted at temperatures of 25°, 75° and 125° C. on specimens randomly selected from Boreholes 209-021-SV1 and 209-030-DIL1. Results from the tests showed that the uniaxial compressive strengths of the specimens from Borehole 209-030-DIL1 were consistently lower than those from Borehole 209-021-SV1 at all test temperatures. Triaxial testing results from previous testing programs (Lau et al., 1988b) showed that the triaxial strengths of the specimens from Borehole 209-030-DIL1 were also consistently lower than those from Borehole 209-021-SV1 at all test temperatures and at all confining pressure levels. It was therefore decided to modify the testing program and divide the program into two parts: one for specimens from Borehole 209-021-SV1 and one for specimens from Borehole 209-030-DIL1. Three sets of tests at three test temperatures were carried out in each part of the test program. The results are summarized in Tables 3 and 4.

6. Results and discussion

6.1 Test results

Tables 3 and 4 summarize the total axial strain at failure, uniaxial compressive strength, tangent Young's modulus and pseudo Young's modulus at 50% of failure load, Poisson's ratio, and failure characteristics of each specimen. Note that axial strains were measured using LVDTs. In those instances where strain gauges were applied, the total axial strains at failure measured using strain gauges and the corresponding values of tangent Young's modulus, pseudo Young's modulus and Poisson's ratio calculated are also given in the tables. Poisson's ratio was determined from the ratio of the circumferential and tangential deformation tangent moduli at 50% of the failure load. The effects of temperature on the strength and elastic properties of the rock samples will be discussed in the following subsections.

Note that the uniaxial compressive strength and Young's moduli of Specimen 209-030-DIL1-2.44 were very low and were therefore not used in the analysis of data.

Stress versus axial strain and stress versus circumferential strain curves for all tests are illustrated in Appendices A and B. These curves were plotted by the use of DATAPLOT curve fitting software. A cubic spline fit was used for this analysis which employed a third degree equation model of the form:

$$\sigma = a_0 + a_1\varepsilon + a_2\varepsilon^2 + a_3\varepsilon^3 \tag{4}$$

where σ = stress

ε = strain

and a_0, a_1, a_2 and a_3 are coefficients

Note that the axial strain was computed by averaging the axial strain data obtained from the three LVDTs.

6.2 Effect of temperature on uniaxial compressive strength

One of the main objectives of these tests was to study the effect of temperature on the uniaxial compressive strength of the rock. The uniaxial compressive strengths of the specimens are shown in Tables 3 and 4, and were plotted against temperature in Figures 1 and 2.

Figure 1 shows that for Borehole 209-021-SV1, there was no change in the mean uniaxial compressive strength when the temperature was raised from 25° to 75° C. At 25° and 75° C, the mean uniaxial compressive strengths were 185.7 MPa (s.d. = 3.5 MPa) and 186.0 MPa (s.d. = 6.9 MPa) respectively. However, a slight decrease in the mean uniaxial compressive strength was observed when the temperature was increased from 75° to 125° C. The mean uniaxial compressive strength decreased from 186.0 MPa at 75° C to 179.7 MPa (s.d. = 2.5 MPa) at 125° C.

For Borehole 209-030-DIL1, Figure 2 shows very little decrease in the mean uniaxial compressive strength when the temperature was increased from 25° to 75° C, but a slight decrease when the temperature was raised from 75° to 125° C. At an ambient room temperature of 25° C, the mean uniaxial compressive strength was 168.7 MPa (s.d. = 7.8 MPa). The mean uniaxial compressive strength decreased from 168.0 MPa

(s.d. = 1.4 MPa) to 162.0 MPa (s.d. = 1.4 MPa) when the temperature increased from 75° to 125° C.

It should be pointed out that rock specimens from Borehole 209-021-SV1 were consistently stronger (approximately 18 MPa) than those from Borehole 209-030-DIL1 at all test temperatures.

6.3 Effect of temperature on axial strain at failure

The total axial strain at failure was found to decrease with increasing temperature. The mean total axial strain for specimens from Borehole 209-021-SV1 decreased from 0.3863% (s.d. = 0.0374%) to 0.3520% (s.d. = 0.0036%) to 0.3407% (s.d. = 0.0059%) when the temperature was raised from 25° to 75° to 125° C. For specimens from Borehole 209-030-DIL1, the mean total axial strain decreased from 0.3607% (s.d. = 0.0412%) to 0.3285% (s.d. = 0.0078%) to 0.3255% (s.d. = 0.0007%) when the temperature increased from 25° to 75° to 125° C.

The axial strains at failure for specimens from Borehole 209-021-SV1 were greater than those for specimens from Borehole 209-030-DIL1.

6.4 Effect of Temperature on tangent Young's modulus

Tangent Young's moduli for the rock specimens were computed at stress levels corresponding to 10%, 20%, 30%, 40%, 50%, 60%, 70%, 80% and 90% of the uniaxial compressive strength and are presented in Tables 5 and 6. The tangent modulus was computed by using Equation 4 to represent the stress versus axial strain curve (see Appendices A and B), solving the equation, and then substituting the axial strain value into the derivative of the equation. The tangent Young's modulus was plotted against normalized axial stress for the three test temperatures in Figures 3 and 4. Normalized axial stress is defined as the ratio of the axial stress to the axial stress at failure. At all three temperature conditions, the tangent modulus increased at a decreasing rate until the nomalized axial stress reached 0.6 and then decreased slowly until failure. This indicates the presence of microcracks in the specimens probably caused by stress relaxation, resulting in lower modulus values at lower stress levels.

Figures 3 and 4 show that temperature had no significant effect on the tangent modulus at any stress level. In Figures 5 and 6, tangent moduli at 50% of failure load and their mean values were plotted versus temperature. No change in the mean value was observed when the temperature was increased from 25° to 75° C. However, a slight

decrease in the mean modulus value was observed when the temperature was raised from 75° to 125° C. The mean tangent modulus for specimens from Borehole 209-021-SV1 decreased from 66.24 GPa (s.d. = 1.24 GPa) at 75° C to 64.20 GPa (s.d = 0.46 GPa) at 125° C. For specimens obtained from Borehole 209-030-DIL1, the mean tangent modulus at 50% of failure load decreased from 61.83 GPa (s.d. = 0.78 GPa) at 75° C to 59.05 GPa (s.d. = 2.13 GPa) at 125° C.

It should be noted that the mean tangent Young's moduli at 50% of failure load for specimens from Borehole 209-021-SV1 were approximately 5 GPa higher than those for specimens from Borehole 209-030-DIL1 at all three test temperatures.

6.5 Effect of temperature on pseudo Young's modulus

Actual stress versus axial strain curves for these specimens are nonlinear (see Appendices A and B). For modelling purposes, these nonlinear curves may be idealized as a series of straight lines joining points corresponding to stress levels of 0.0, 0.1, 0.2, 0.3, 0.4, 0.5, 0.6, 0.7, 0.8, 0.9 and 1.0 times the failure axial stress. The slope of the linear stress-strain curve during each stress interval is defined as the pseudo Young's modulus. The pseudo Young's moduli of the rock samples are presented in Tables 7 and 8. In general, the pseudo moduli were lower than the tangent moduli at stress levels below 0.6 times the failure stress, particularly at very low stress levels, but higher than the tangent moduli at stress levels above 0.6 times the failure stress.

The plots of the pseudo Young's modulus versus normalized axial stress for the samples at temperatures of 25°, 75° and 125° C are shown in Figures 7 and 8. The patterns are very similar to those of the plots of the tangent Young's modulus versus normalized axial stress (see Figs. 3 and 4), and illustrate that temperature has no significant effect on pseudo Young's modulus. Pseudo Young's moduli at 50% of failure load and their mean values were plotted in Figures 9 and 10. Again, no change in the mean value was observed when the temperature was increased from 25° to 75° C, and a slight decrease was observed when the temperature was raised from 75° to 125° C. The mean pseudo modulus for specimens obtained from Borehole 209-021-SV1 decreased from 65.31 GPa (s.d. = 1.37 GPa) at 75° C to 63.13 GPa (s.d. = 0.43 GPa) at 125° C. For specimens from Borehole 209-030-DIL1, the mean modulus value decreased from 60.81 GPa (s.d. = 0.78 GPa) at 75° C to 57.78 GPa (s.d. = 2.36 GPa) at 125° C.

The mean pseudo Young's modulus at 50% of failure load of the specimens from Borehole 209-021-SV1 were also approximately 5 GPa higher than those from Borehole 209-030-DIL1.

6.6 Effect of temperature on Poisson's ratio

The Poisson's ratios (see Tables 3 and 4) and the mean values obtained from the tests were plotted versus temperature in Figures 11 and 12. The plots show that the mean Poisson's ratio decreased when temperature increased from 25° to 75° C. However, there was no change in Poisson's ratio when the temperature was raised from 75° to 125° C. The mean Poisson's ratios for specimens from Borehole 209-021-SV1 at test temperatures of 25°, 75° and 125° C were 0.38 (s.d. = 0.16), 0.27 (s.d. = 0.02) and 0.27 (s.d. = 0.01) respectively, and those from Borehole 209-030-DIL1 were 0.29 (s.d.= 0.02), 0.25 (s.d. = 0.01) and 0.25 (s.d. = 0.01) respectively.

6.7 Effect of temperature on strength properties

The strength properties of intact rock material can be expressed in terms of the Hoek and Brown failure criterion. The empirical relationship developed by Hoek and Brown (1980) between the principal stresses associated with the failure of a rock are given as follows:

$$\sigma_1 = \sigma_3 + \sqrt{m\sigma_c\sigma_3 + s{\sigma_c}^2} \tag{5}$$

where σ_1 = major principal stress at failure
σ_3 = minor principal stress applied to the rock sample
σ_c = uniaxial compressive strength of the intact rock material in the specimen
m and s are constants

The values of m and s depend on the properties of the rock and the extent to which the rock has been broken before being subjected to principal stresses σ_1 and σ_3. For an intact rock, $s = 1$, and the uniaxial compressive strength σ_c and the material constant m can be computed by using the following equations:

$$\sigma_c^2 = \frac{\sum y_i}{n} - \left[\frac{\sum x_i y_i - \frac{\sum x_i \sum y_i}{n}}{\sum x_i^2 - \frac{(\sum x_i)^2}{n}}\right]\frac{\sum x_i}{n} \tag{6}$$

$$m = \frac{1}{\sigma_c}\left[\frac{\sum x_i y_i - \frac{\sum x_i \sum y_i}{n}}{\sum x_i^2 - \frac{(\sum x_i)^2}{n}}\right] \tag{7}$$

where $x = \sigma_3$

$y = (\sigma_1 - \sigma_3)^2$

n = total number of data pairs x_i and y_i

The coefficient of determination r^2 is given by:

$$r^2 = \frac{\left[\sum x_i y_i - \frac{\sum x_i \sum y_i}{n}\right]^2}{\left[\sum x_i^2 - \frac{(\sum x_i)^2}{n}\right]\left[\sum y_i^2 - \frac{(\sum y_i)^2}{n}\right]} \tag{8}$$

The closer the value of r^2 is to 1.00, the better the fit between Equation 5 and the triaxial test data is.

To facilitate the development of the Hoek and Brown failure envelopes for these samples, the results of previous triaxial tests on samples from Boreholes 209-021-SV1 and 209-030-DIL1 (Lau et al., 1988b) were included in the analysis using Equation 5. The Hoek and Brown failure envelopes are shown in Figures 13 to 17. The values of m and r^2 as well as the computed uniaxial compressive strength, σ_c, are shown in Tables 9 and 10. The coefficient of determination, r^2, ranged from 0.9924 to 0.9968, indicating that the fit of Equation 5 to the data was good.

From Table 9, it can be seen that for Borehole 209-021-SV1, σ_c decreased from 201 to 186 MPa as the temperature increased from 75° to 125° C. There was little change in σ_c when the temperature was raised from 25° to 75° C. The m value decreased from 39.03 to 36.50 as the temperature increased from 25° to 75° C. However, there was virtually no change in the value of m when the temperature was raised from 75° to 125° C.

For samples from Borehole 209-030-DIL1 (see Table 10), when the temperature increased from 75° to 125° C, the m value increased from 34.57 to 36.09, but very little change (from 175 to 174 MPa) in σ_c was observed. Note that no triaxial data was available for the computation of the values of σ_c and m at 25° C.

It should be noted that the values of σ_c obtained from Borehole 209-030-DIL1 were significantly lower than those from Borehole 209-021-SV1, indicating again that

the rock specimens from Borehole 209-021-SV1 were stronger than those from Borehole 209-030-DIL1.

The values of σ_c and m computed by Lau et al. (1988b) for the same type of rock at temperatures of 75° and 125° C, in the absence of high temperature uniaxial compressive strength data, were 231 MPa and 26.31, and 200 MPa and 31.27 respectively. With high temperature uniaxial compressive strength data available, σ_c became lower and m became higher than previous values.

The effect of temperature on the values of σ_c and m is still not clear. It seems that σ_c decreased when the temperature was raised from 75° to 125° C. The m value might increase or decrease with increasing temperature. However, the change was small in either case.

Hoek and Brown also suggest that the relationship between the shear and normal stresses (τ and σ) and the principal stresses at failure can be expressed as follows:

$$\sigma = \sigma_3 + \frac{\tau_m^2}{\tau_m + m\sigma_c/8} \tag{9}$$

$$\tau = (\sigma - \sigma_3)\sqrt{1 + m\sigma_c/4\tau_m} \tag{10}$$

where $\tau_m = \frac{1}{2}(\sigma_1 - \sigma_3)$

By substituting successive pairs of σ_1 and σ_3 into Equations 9 and 10, a Mohr failure envelope can be generated.

The Mohr failure envelopes and the Mohr circles for the rock samples were plotted in Figures 18 to 22. In each plot, results from tests conducted under the same temperature condition were presented. Note that for each confining pressure level, only the mean Mohr circle was plotted. From those figures, it can be seen that the failure envelopes generated fit very well with the Mohr circles. The angles of internal friction and the cohesive strengths of the rock samples, defined by the tangents to the points of intersections of the failure envelopes and the Mohr circles are shown in Tables 11 and 12. The angle of internal friction was found to decrease but the cohesive strength to increase with increasing confining pressure at all test temperatures, as expected. No significant change in the angle of internal friction and the cohesive strength of the samples with increasing temperature was observed. The angles of internal friction of specimens

from Borehole 209-021-SV1 were found to be slightly larger than those from Borehole 209-030-DIL1.

7. Conclusions

The results of these tests have provided some high temperature uniaxial compressive strength data as well as some insight into the behaviour of the grey granite at the 240 level of the AECL Underground Research Laboratory. It has also been found that the strength and elastic properties of URL grey granite are site-specific. Samples from Borehole 209-021-SV1 were stronger and stiffer than those from Borehole 209-030-DIL1. From the results, the following observations can be reached:

No change in the mean uniaxial compressive strength was observed when the temperature was raised from 25° to 75° C. However, the mean uniaxial compressive strength decreased by approximately 6 MPa when the temperature increased from 75° to 125° C.

The axial strain at failure decreased with increasing temperature.

Temperature had little effect on the tangent Young's modulus and the pseudo Young's modulus. Only slight decreases of less than 3.2 GPa in the mean modulus values were observed when the temperature was raised from 75° to 125° C.

Plots of tangent Young's modulus and pseudo Young's modulus versus normalized axial stress indicate the presence of microcracks in the specimens, resulting in lower modulus values at lower stress levels.

The mean Poisson's ratio was found to decrease when the temperature increased from 25° to 75° C, but no change in Poisson's ratio was observed when the temperature was raised from 75° to 125° C.

The strength properties of the rock samples were expressed in terms of the Hoek and Brown failure criterion. Triaxial strength data from previous high temperature triaxial tests were also included in the analysis. The results show that with the addition of high temperature uniaxial compressive strength data, the predicted uniaxial compressive strength of the intact rock material σ_c becomes lower and the material constant m becomes higher. The effect of temperature on σ_c and m is still not clear. The value of σ_c appeared to decrease when the temperature was raised from 75° to 125° C. The value of m might increase or decrease with increasing temperature, although the change was small.

The angles of internal friction and the cohesive strengths of the samples derived from the plots of Mohr failure envelopes and Mohr circles appeared to be insensitive to an increase in temperature.

8. Recommendations

Since the strength and elastic properties of rock specimens can vary significantly from one location to another at the URL, it is recommended that samples in any testing program be obtained from the same location at the URL, that is from a limited section of a borehole, so that changes in the strength and elastic properties due to location are not mistaken for changes in properties with temperature.

The effect of temperature on the values of σ_c and m is not clear. More tests should be conducted to address this issue.

At present, only two types of rock (grey granite and pink granite) and one size (NQ) of specimens have been tested at high temperature. High temperature uniaxial and triaxial tests should be carried out on other types of rock found at the URL site to better understand the response of the rock mass to changes in stress and temperature. Tests should also be conducted on specimens of other sizes to investigate the scale effects on the thermal-mechanical properties of the URL rock samples in order to better relate the laboratory determined thermal-mechanical properties to in situ condtions.

Acknowledgements

The authors wish to express their thanks to R. Jackson and G.E. Larocque of CANMET for reviewing this report and making several helpful suggestions. Gratitude is expressed to J. Folta of CANMET and G.P. Hunter and P.A. Tibble, co-op students from the University of Waterloo, for the preparation of specimens and for carrying out the compression wave and shear wave velocities measurements.

References

Annor, A., Miles, P., Kapeller, F. and Larocque, G. (1981), "High temperature and pressure triaxial compression tests on rock samples from Pinawa and the Creighton Mine", Atomic Energy of Canada Limited Technical, Record TR-158, 51 p.

Annor, A. and Jackson, R. (1985), "Mechanical properties of rock samples from the Lac du Bonnet Batholith, Manitoba", Division Report M&ET/MRL 85-41(TR), CANMET, Energy, Mines and Resources Canada, 101 p.

Annor, A. and Jackson, R. (1987), "Mechanical, thermomechanical and joint properties of rock samples from the Lac du Bonnet Batholith, Manitoba", in Geotechnical studies at Whiteshell Research Area (RA-3) (edited by Katsube, T.J. and Hume, J.P.), Division Report MRL 87-52(TR), CANMET, Energy, Mines and Resources Canada, 232 p.

Brown, E.T. (1981), "Rock characterization testing and monitoring, ISRM suggested methods", International Society for Rock Mechanics, the Commission on Testing Methods, Pregamon, 211 p.

Gorski, B. (1987), "Post-failure uniaxial strength determinations using a servo-hydraulic test system", Division Report MRL 87-33(INT), CANMET, Energy, Mines and Resources Canada, 77 p.

Gyenge, M. and Herget, G. (1977), "Pit slop manual supplement 3-2 - laboratory tests for design parameters", CANMET, CANMET Report 77-26, 74 p.

Gyenge, M. and Ladanyi, B. (1977), "Pit slope manual supplement 3-5 - sampling and specimen preparation", CANMET, CANMET Report 77-29, 30 p.

Hoek, E. and Brown, E.T. (1980), "Underground excavations in rock", The institution of Mining and Metallurgy, London, 527 p.

Jackson, R. (1984), "Summary of mechanical properties of Lac du Bonnet and Eye-Dashwa specimens", Division Report MRP/MRL 84-85(TR), CANMET, Energy, Mines and Resources Canada, 48 p.

Lau, J.S.O., Jackson, R. and Gorski, B. (1988a), "High temperature triaxial tests on rock samples from Borehole URL-5, Lac du Bonnet, Manitoba", Division Report MRL 88-90(TR), CANMET, Energy, Mines and Resources Canada, 86 p.

Lau, J.S.O., Jackson, R. and Gorski, B. (1988b), "High temperature triaxial tests on rock samples from Boreholes 209-021-SV1 and 209-030-DIL1, Lac du Bonnet, Manitoba", Division Report MRL 88-112(TR), CANMET, Energy, Mines and Resources Canada, 57 p.

MTS Systems Corporation (1986), "Operation manual for 815 rock mechanics test systems", MTS Systems Corp., Minneapolis, Minnesota, U.S.A.

Simmons, G.R. and Soonawala, N.M. (1982), "Underground research laboratory experimental program", Atomic Energy of Canada Limited Technical Record, TR-153, 126 p.

Terrametrics (1980), "Instruction manual - sonic velocity equipment", Terrametrics, Inc., Golden, Colorado, U.S.A., 17 p.

Table 1. Dimensions, densities and dynamic elastic properties of rock samples from Borehole 209-021-SV1.

Specimen identification	Length (mm)	Diameter (mm)	Bulk density (Mg/m^3)	P-wave velocity (km/s)	S-wave velocity (km/s)	Dynamic Young's modulus (GPa)	Dynamic shear modulus (GPa)	Dynamic Poisson's ratio
209-021-SV1-4.11	105.65	45.07	2.63	5.187	2.949	57.70	22.88	0.26
209-021-SV1-4.23	106.98	45.09	2.63	4.839	2.795	51.34	20.54	0.25
209-021-SV1-4.34	105.80	45.10	2.63	4.998	2.895	55.01	22.05	0.25
209-021-SV1-4.45	108.06	45.04	2.63	4.711	2.732	48.93	19.62	0.25
209-021-SV1-4.62	105.86	45.20	2.62	4.739	2.761	49.65	19.97	0.24
209-021-SV1-4.73	108.44	45.16	2.63	4.880	2.814	52.12	20.83	0.25
209-021-SV1-4.84	106.43	45.09	2.64	5.300	2.793	53.86	20.59	0.31
209-021-SV1-4.96	106.49	45.09	2.64	5.515	2.809	55.20	20.83	0.32
209-021-SV1-5.40	112.83	45.23	2.62	5.103	2.941	56.70	22.66	0.25
Mean				5.030	2.832	53.39	21.11	0.26
Standard deviation				0.270	0.078	3.07	1.16	0.03

Table 2. Dimensions, densities and dynamic elastic properties of rock samples from Borehole 209-030-DIL1.

Specimen identification	Length (mm)	Diameter (mm)	Bulk density (Mg/m^3)	P-wave velocity (km/s)	S-wave velocity (km/s)	Dynamic Young's modulus (GPa)	Dynamic shear modulus (GPa)	Dynamic Poisson's ratio
209-030-DIL1-2.44	107.94	44.96	2.63	4.687	2.763	49.55	20.08	0.23
209-030-DIL1-2.55	107.28	45.00	2.63	4.668	2.751	49.13	19.91	0.23
209-030-DIL1-2.66	105.64	44.89	2.64	4.828	2.740	50.03	19.81	0.26
209-030-DIL1-2.77	109.29	44.87	2.64	4.505	2.677	46.44	18.92	0.23
209-030-DIL1-2.89	111.96	45.06	2.62	4.742	2.775	50.03	20.18	0.24
209-030-DIL1-3.57	108.84	44.92	2.63	4.531	2.632	45.37	18.21	0.25
209-030-DIL1-3.69	108.22	44.88	2.63	4.448	2.615	44.46	17.99	0.24
209-030-DIL1-3.80	104.44	44.88	2.63	4.636	2.674	47.03	18.80	0.25
Mean				4.631	2.703	47.76	19.24	0.24
Standard deviation				0.128	0.062	2.21	0.87	0.01

Table 3. Results of ambient temperature and high temperature uniaxial tests on rock samples from Borehole 209-021-SV1.

Specimen	Length (mm)	Diameter (mm)	Temp. (deg C.)	Total Axial Strain (%)	Uniaxial Compressive Strength (MPa)	Tangent Young's Modulus (GPa)	Pseudo Young's Modulus (GPa)	Poisson's Ratio	Failure characteristics
209-021-SV1-4.11	105.65	45.07	25	0.418	189	66.25	65.29	0.36	multiple vertical cracks
				0.312*		66.25*	65.55*	0.36*	
209-021-SV1-4.23	106.98	45.09	25	0.396	182	64.23	63.12	0.23	multiple vertical cracks
				0.297*		66.95*	66.51*	0.24*	
209-021-SV1-5.40	112.83	45.23	25	0.345	186	66.09	65.31	0.54	multiple vertical cracks
				0.284*		69.52*	68.84*	0.56*	
209-021-SV1-4.34	105.80	45.10	75	0.355	178	64.94	63.82	0.25	multiple vertical cracks
209-021-SV1-4.45	108.06	45.04	75	0.353	190	67.40	66.51	0.28	multiple vertical cracks
209-021-SV1-4.96	106.49	45.09	75	0.348	190	66.38	65.59	0.29	multiple vertical cracks
209-021-SV1-4.62	105.86	45.20	125	0.345	180	64.73	63.62	0.28	multiple vertical cracks
209-021-SV1-4.73	108.44	45.16	125	0.334	177	63.92	62.82	0.28	multiple vertical cracks
209-021-SV1-4.84	106.43	45.09	125	0.343	182	63.96	62.96	0.26	multiple vertical cracks

*computed from strain gauge measurements

Table 4. Results of ambient temperature and high temperature uniaxial tests on rock samples from Borehole 209-030-DIL1.

Specimen	Length (mm)	Diameter (mm)	Temp. (deg C.)	Total Axial Strain (%)	Uniaxial Comp. Strength (MPa)	Tangent Young's Modulus (GPa)	Pseudo Young's Modulus (GPa)	Poisson's Ratio	Failure characteristics
209-030-DIL1-2.44	107.94	44.96	25	0.333	145	54.58	53.08	0.32	multiple cracks, bottom wedge
				0.324*		53.73*	52.84*	0.31*	
209-030-DIL1-2.77	109.29	44.87	25	0.341	171	62.45	61.51	0.28	multiple vertical cracks
				0.303*		65.40*	64.85*	0.29*	
209-030-DIL1-2.89	111.96	45.06	25	0.333	160	59.84	58.68	0.31	multiple cracks, bottom wedge
				0.315*		60.98*	60.30*	0.32*	
209-030-DIL1-3.57	108.84	44.92	25	0.408	175	61.52	60.41	0.29	multiple vertical cracks
				0.311*		65.14*	64.63*	0.31*	
209-030-DIL1-2.55	107.28	45.00	75	0.334	167	61.27	60.25	0.24	multiple vertical cracks
209-030-DIL1-3.69	108.22	44.88	75	0.323	169	62.38	61.36	0.25	multiple vertical cracks
209-030-DIL1-2.66	105.64	44.89	125	0.325	163	60.55	59.45	0.26	multiple vertical cracks
209-030-DIL1-3.80	104.44	44.88	125	0.326	161	57.54	56.11	0.24	multiple cracks, top wedge

*computed from strain gauge measurements

Table 5. Tangent Young's moduli of rock samples from Borehloe 209-021-SV1.

Specimen Identification	Temp. (deg C.)	Tangent Young's Modulus (GPa)								
		0.1	0.2	0.3	0.4	0.5	0.6	0.7	0.8	0.9
209-021-SV1-4.11	25	37.24	51.03	59.21	63.98	66.25	66.36	64.33	59.86	50.36
209-021-SV1-4.11*		42.47	54.99	61.16	64.59	66.25	66.33	64.84	61.61	87.05
209-021-SV1-4.23	25	37.96	50.07	57.25	61.73	64.23	65.03	64.23	61.75	54.77
209-021-SV1-4.23*		45.14	56.87	62.93	65.80	66.95	66.50	64.40	60.42	69.50
209-021-SV1-5.40	25	39.82	53.35	60.52	64.25	66.09	66.30	64.89	61.73	54.72
209-021-SV1-5.40*		44.86	58.16	64.86	67.94	69.52	69.83	68.88	66.61	91.77
209-021-SV1-4.34	75	38.49	50.93	57.99	62.44	64.94	65.78	65.05	62.68	54.93
209-021-SV1-4.45	75	41.45	54.12	61.11	65.31	67.40	67.61	65.98	62.32	54.29
209-021-SV1-4.96	75	44.93	55.92	61.21	64.57	66.38	66.79	65.85	63.47	56.44
209-021-SV1-4.62	125	38.74	50.49	57.73	62.24	64.73	65.51	64.65	62.07	54.52
209-021-SV1-4.73	125	39.65	50.84	57.31	61.48	63.92	64.89	64.46	62.61	55.81
209-021-SV1-4.84	125	39.53	50.95	57.56	61.69	63.96	64.62	63.74	61.22	54.55

*computed from strain gauge measurements

Table 6. Tangent Young's moduli of rock samples from Borehole 209-030-DIL1.

Specimen Identification	Temp. (deg C.)	Tangent Young's Modulus (GPa)								
		0.1	0.2	0.3	0.4	0.5	0.6	0.7	0.8	0.9
209-030-DIL1-2.44	25	27.82	39.19	46.33	51.28	54.58	56.12	56.08	54.47	48.38
209-030-DIL1-2.44*		30.22	41.10	47.57	51.62	53.73	53.84	51.96	48.10	44.06
209-030-DIL1-2.77	25	36.05	49.04	56.27	60.31	62.45	63.04	62.14	59.66	52.69
209-030-DIL1-2.77*		39.68	53.08	60.30	63.98	65.40	64.89	62.38	57.51	57.25
209-030-DIL1-2.89	25	32.71	45.33	52.70	57.25	59.84	60.81	60.28	58.19	51.94
209-030-DIL1-2.89*		35.81	48.09	55.16	59.25	60.98	60.56	57.93	52.87	48.74
209-039-DIL1-3.57	25	31.76	45.47	53.96	58.96	61.52	62.06	60.62	57.01	49.00
209-030-DIL1-3.57*		43.01	54.54	60.61	63.83	65.14	64.67	62.37	57.97	57.27
209-030-DIL1-2.55	75	35.99	48.38	55.13	59.00	61.27	62.17	61.79	60.08	54.92
209-030-DIL1-3.69	75	37.73	49.43	55.96	60.07	62.38	63.12	62.39	60.10	54.60
209-030-DIL1-2.66	125	34.63	46.65	53.72	58.08	60.55	61.45	60.85	58.70	53.10
209-030-DIL1-3.80	125	37.21	46.36	50.94	54.59	57.54	59.91	61.78	63.21	57.36

*computed from strain gauge measurements

Table 7. Pseudo Young's moduli of rock samples from Borehole 209-021-SV1.

Specimen Identification	Temp. (deg C.)	Pseudo Young's Modulus (GPa)								
		0.1	0.2	0.3	0.4	0.5	0.6	0.7	0.8	0.9
209-021-SV1-4.11	25	20.29	44.34	55.38	61.80	65.29	66.48	65.52	62.30	55.84
209-021-SV1-4.11*		26.71	49.21	58.38	63.02	65.55	66.42	65.72	63.37	66.25
209-021-SV1-4.23	25	20.30	44.34	53.85	59.64	63.12	64.76	64.77	63.13	59.19
209-021-SV1-4.23*		32.52	51.42	60.20	64.51	66.51	66.86	65.59	62.56	60.49
209-021-SV1-5.40	25	27.15	47.02	57.23	62.55	65.31	66.33	65.73	63.46	58.88
209-021-SV1-5.40*		33.46	52.00	61.85	66.55	68.84	69.78	69.46	67.86	74.91
209-021-SV1-4.34	75	26.75	45.17	54.65	60.37	63.82	65.49	65.55	64.01	59.86
209-021-SV1-4.45	75	28.07	48.34	57.82	63.38	66.51	67.65	66.95	64.32	59.03
209-021-SV1-4.96	75	30.45	51.30	58.71	63.02	65.59	66.70	66.43	64.78	60.93
209-021-SV1-4.62	125	29.95	44.87	54.31	60.14	63.62	65.25	65.21	63.50	59.21
209-021-SV1-4.73	125	30.00	45.67	54.24	59.53	62.82	64.52	64.79	63.66	60.21
209-021-SV1-4.84	125	29.74	45.66	54.44	59.78	62.96	64.42	64.31	62.62	58.65

*computed from strain gauge measurements

Table 8. Pseudo Young's moduli of rock samples from Borehole 209-030-DIL1.

Specimen Identification	Temp. (deg C.)	Pseudo Young's Modulus (GPa)								
		0.1	0.2	0.3	0.4	0.5	0.6	0.7	0.8	0.9
209-030-DIL1-2.44	25	18.79	33.72	42.89	48.92	53.08	55.49	56.23	55.41	52.02
209-030-DIL1-2.44*		22.32	35.92	44.51	49.73	52.84	53.95	53.07	50.11	46.03
209-030-DIL1-2.77	25	24.35	42.92	52.90	58.47	61.51	62.87	62.71	61.03	56.98
209-030-DIL1-2.77*		28.19	46.80	56.98	62.36	64.85	65.31	63.80	60.14	56.74
209-030-DIL1-2.89	25	21.81	39.33	49.22	55.14	58.68	60.45	60.67	59.37	55.71
209-030-DIL1-2.89*		26.14	42.28	51.85	57.38	60.30	60.95	59.43	55.51	50.57
209-030-DIL1-3.57	25	17.95	38.61	49.96	56.65	60.41	61.95	61.50	58.99	53.60
209-030-DIL1-3.57*		30.83	49.17	57.86	62.38	64.63	65.05	63.67	60.34	56.36
209-030-DIL1-2.55	75	25.55	42.57	52.01	57.19	60.25	61.83	62.09	61.05	58.30
209-030-DIL1-3.69	75	27.46	44.03	52.87	58.16	61.36	62.87	62.88	61.38	57.80
209-030-DIL1-2.66	125	26.09	40.94	50.38	56.05	59.45	61.12	61.27	59.91	56.57
209-030-DIL1-3.80	125	29.48	42.30	48.70	52.81	56.11	58.76	60.88	62.53	61.71

*computed from strain gauge measurements

Table 9. Values of σ_c, m, s and r^2 obtained from Borehole 209-021-SV1.

Test Temperature (°C.)	Number of Samples n	Estimated Uniaxial Compressive Strength σ_c (MPa)	m	s	r^2
25	9	198	39.03	1.00	0.9943
75	7	201	36.50	1.00	0.9924
125	6	186	36.66	1.00	0.9964

Table 10. Values of σ_c, m, s and r^2 obtained from Borehole 209-030-DIL1.

Test Temperature (°C.)	Number of Samples n	Estimated Uniaxial Compressive Strength σ_c (MPa)	m	s	r^2
75	4	175	34.57	1.00	0.9957
125	5	174	36.09	1.00	0.9968

Table 11. Results of Mohr's circle analysis for Borehole 209-021-SV1.

Confining pressure (MPa)	Test temperature (°C)	Number of samples	Angle of internal friction	Cohesive strength (MPa)
0.0	25	3	68°	22
	75	3	68°	20
	125	3	66°	21
3.5	25	2	66°	24
	75	2	64°	25
	125	1	64°	22
17.0	25	2	55°	46
	75	1	54°	48
	125	1	54°	43
35.0	25	2	48°	70
	75	1	47°	70
	125	1	48°	64

Table 12. Results of Mohr's circle analysis for Borehole 209-030-DIL1.

Confining pressure (MPa)	Test temperature (°C)	Number of samples	Angle of internal friction	Cohesive strength (MPa)
0.0	75 125	2 2	66° 67°	20 17
3.5	125	1	63°	23
17.0	75 125	1 1	52° 52°	44 44
35.0	75 125	1 1	46° 45°	65 68

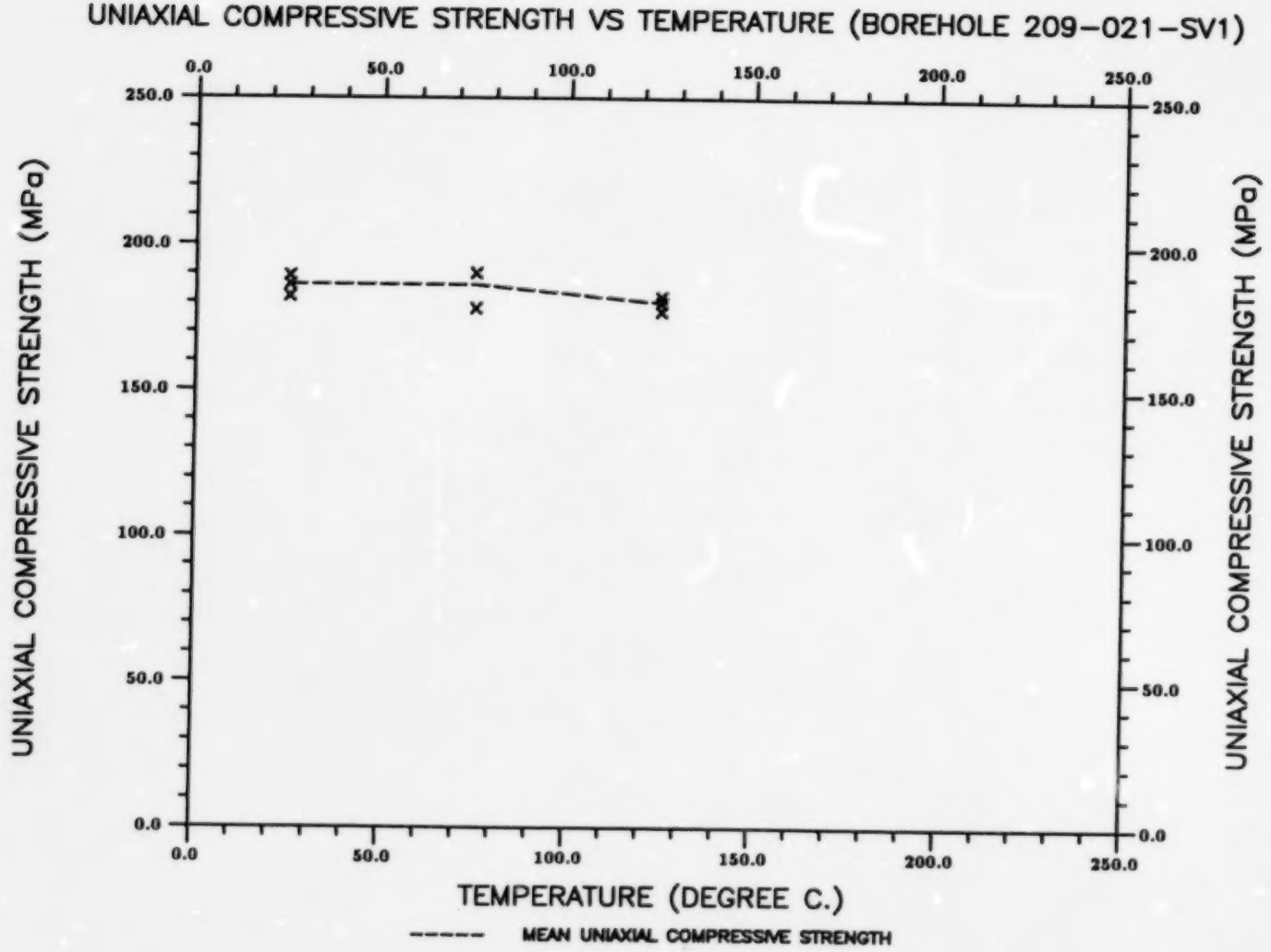

Figure 1. Plot of uniaxial compressive strength versus temperature for Borehole 209-021-SV1.

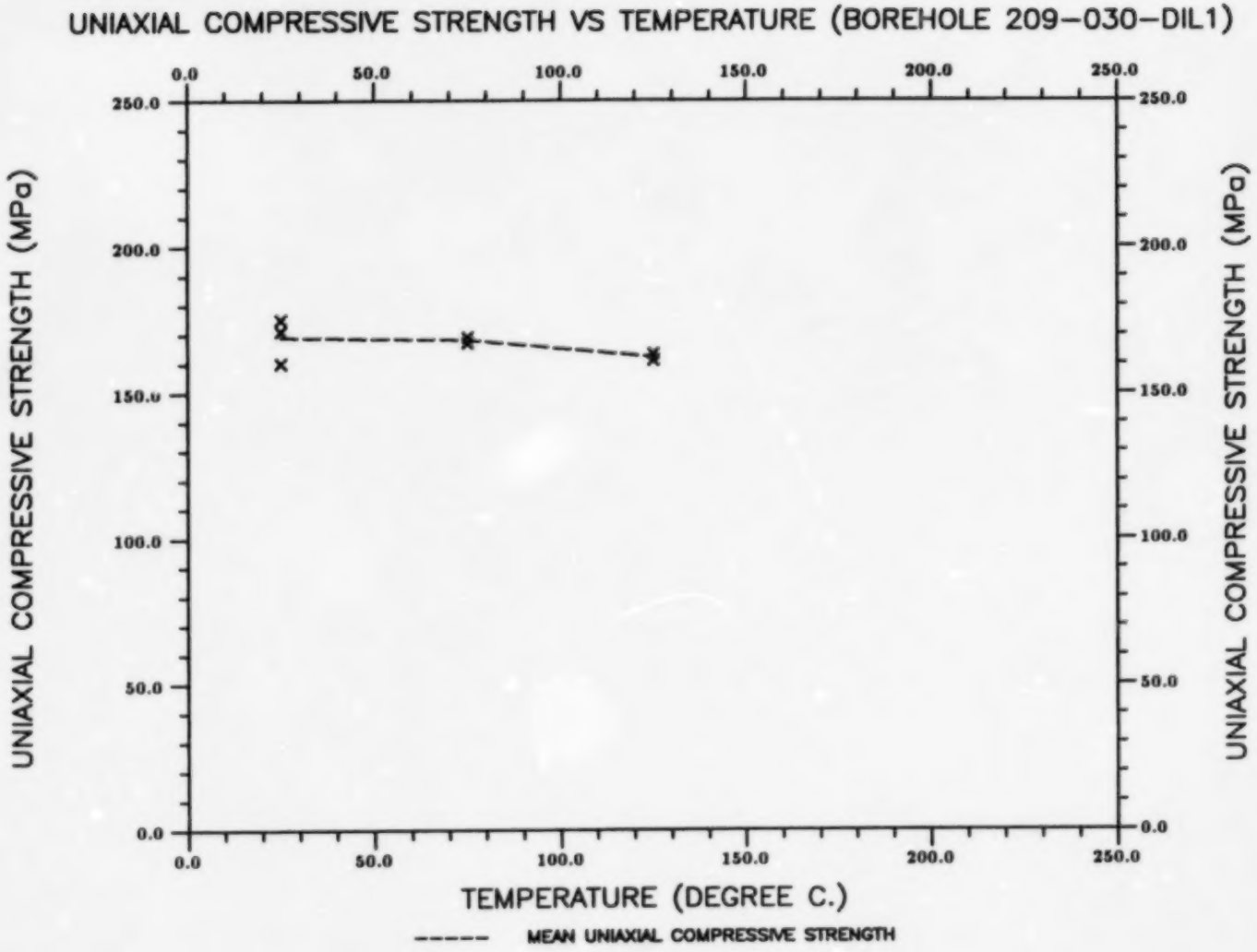

Figure 2. Plot of uniaxial compressive strength versus temperature for Borehole 209-030-DIL1.

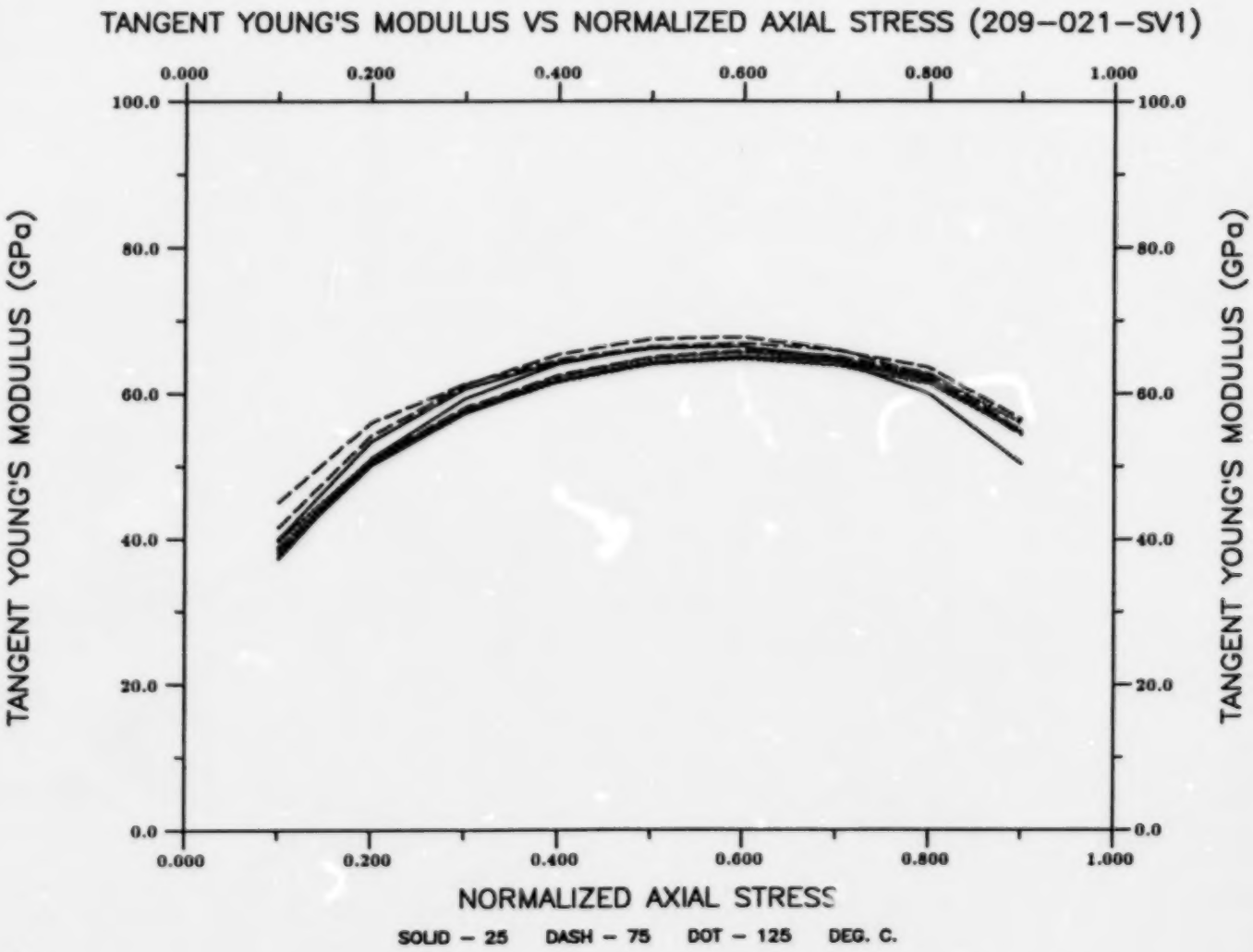

Figure 3. Plots of tangent Young's modulus versus normalized axial stress for Borehole 209-021-SV1.

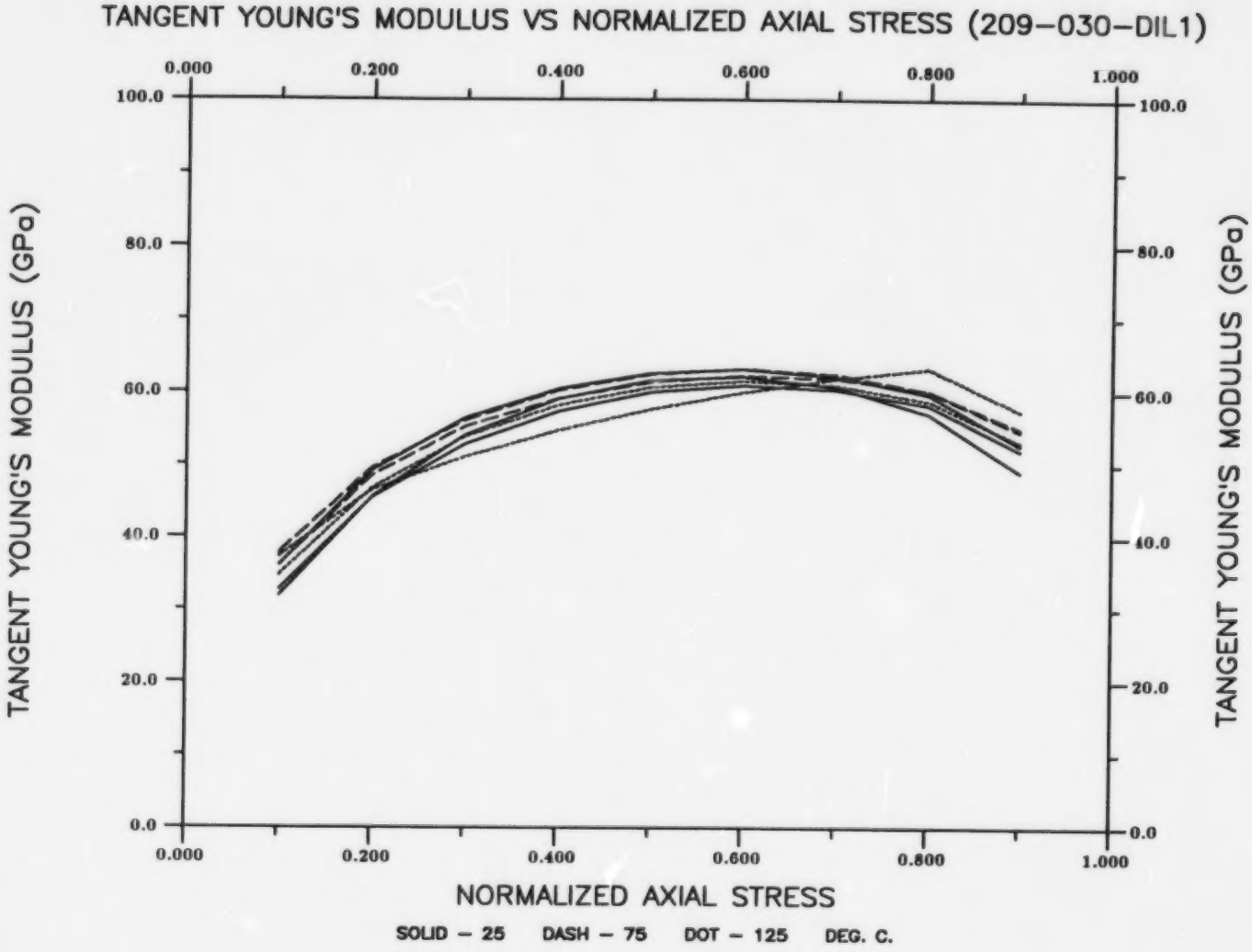

Figure 4. Plots of tangent Young's modulus versus normalized axial stress for Borehole 209-030-DIL1.

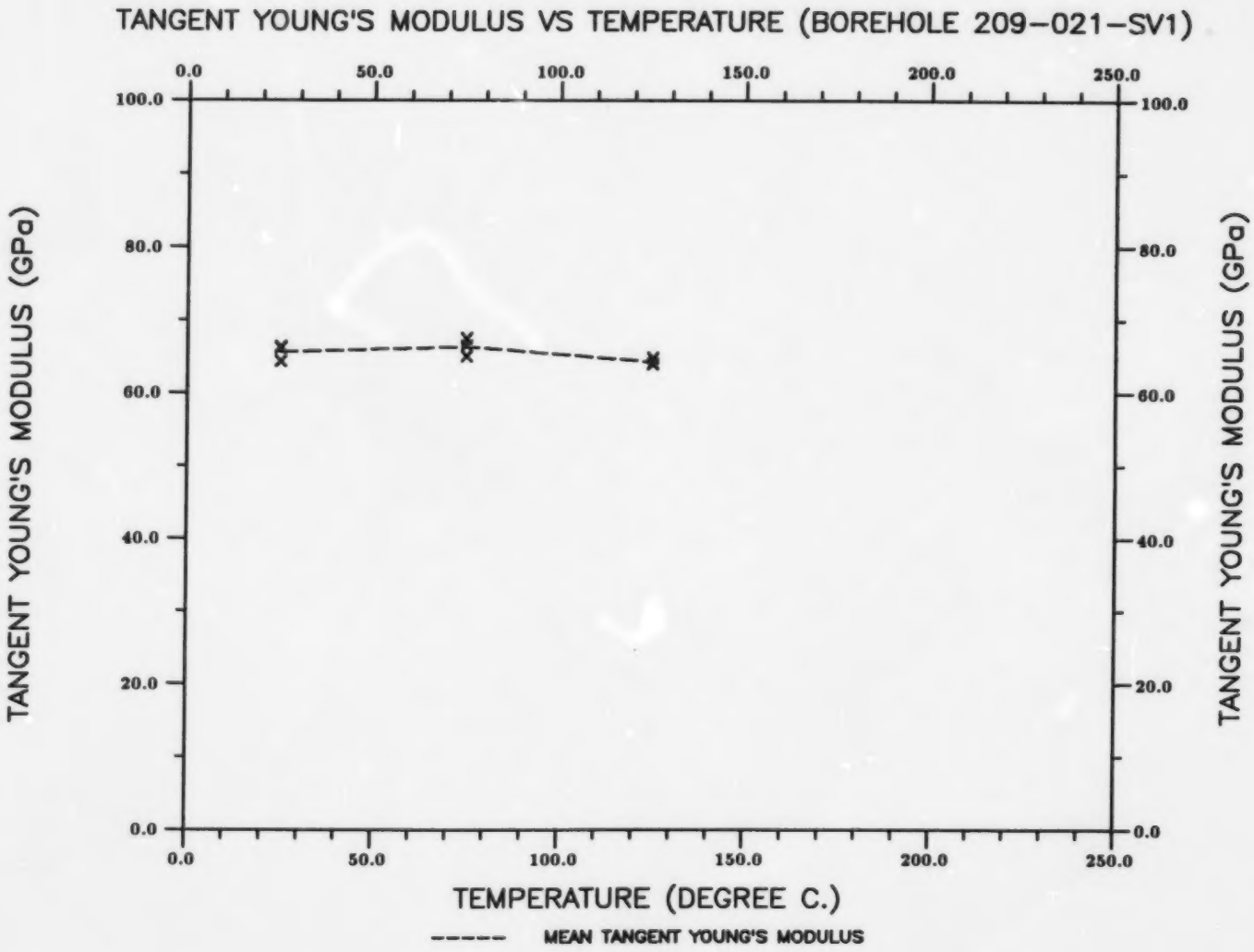

Figure 5. Plot of tangent Young's modulus versus temperature for Borehole 209-021-SV1.

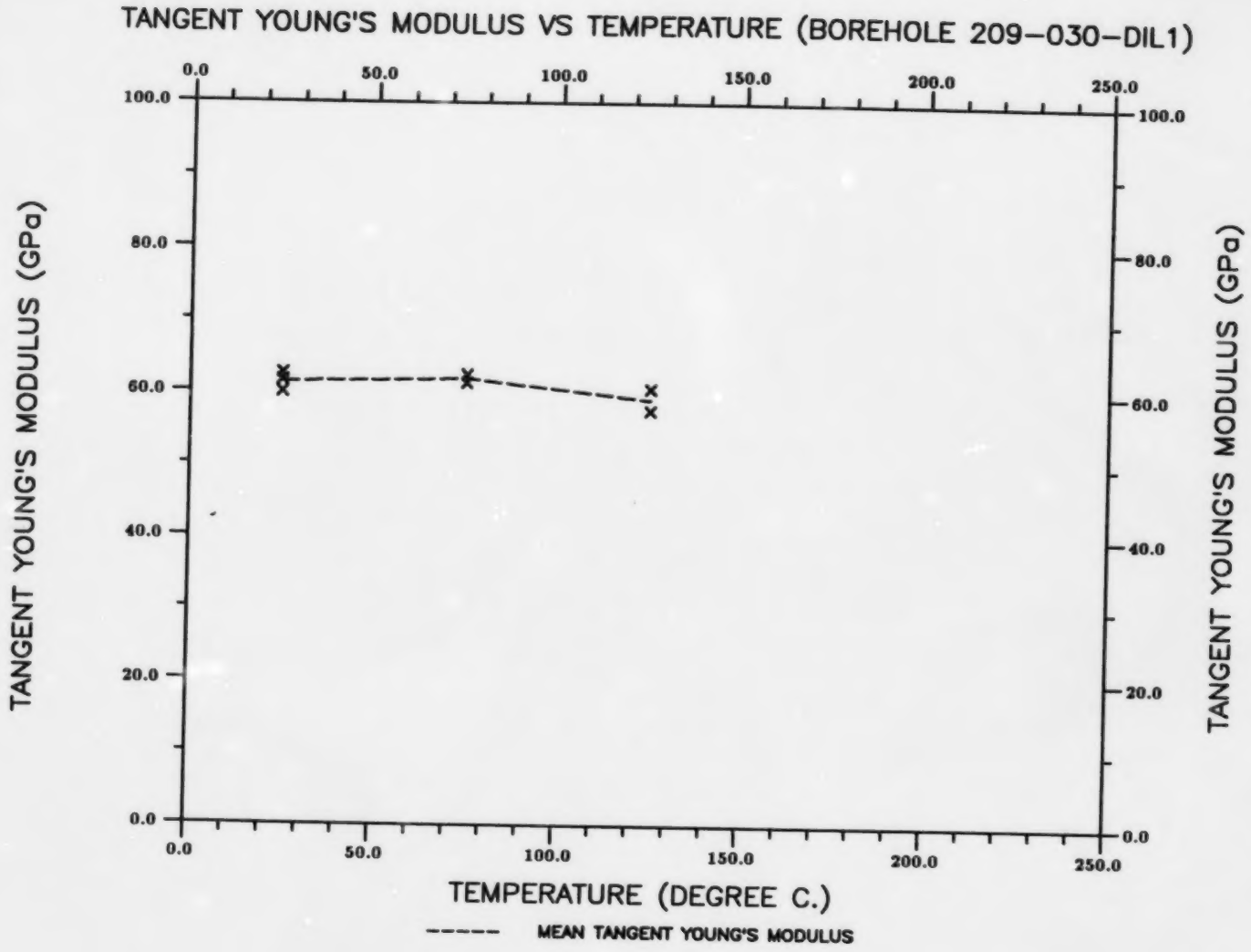

Figure 6. Plot of tangent Young's modulus versus temperature for Borehole 209-030-DIL1.

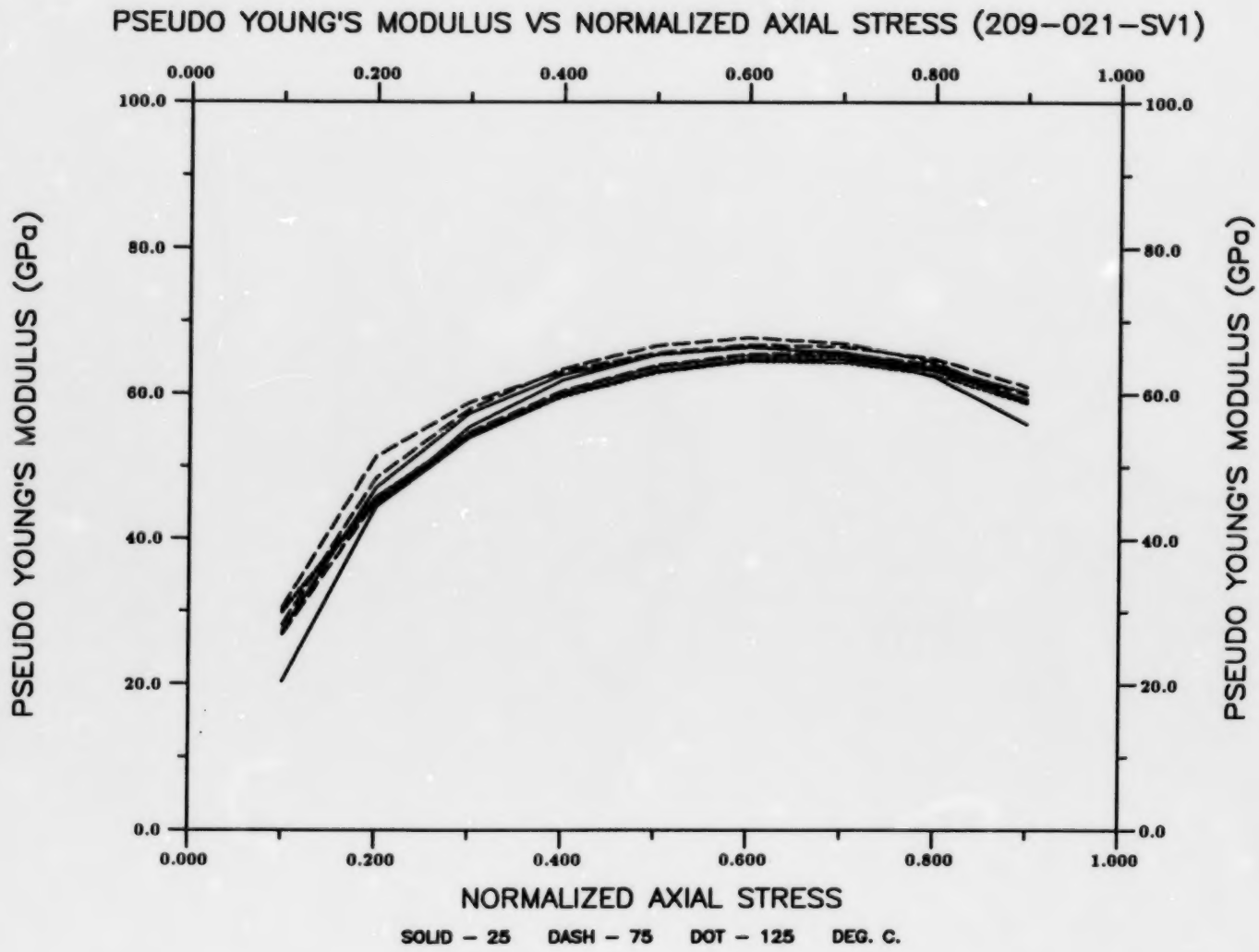

Figure 7. Plots of pseudo Young's modulus versus normalized axial stress for Borehole 209-021-SV1.

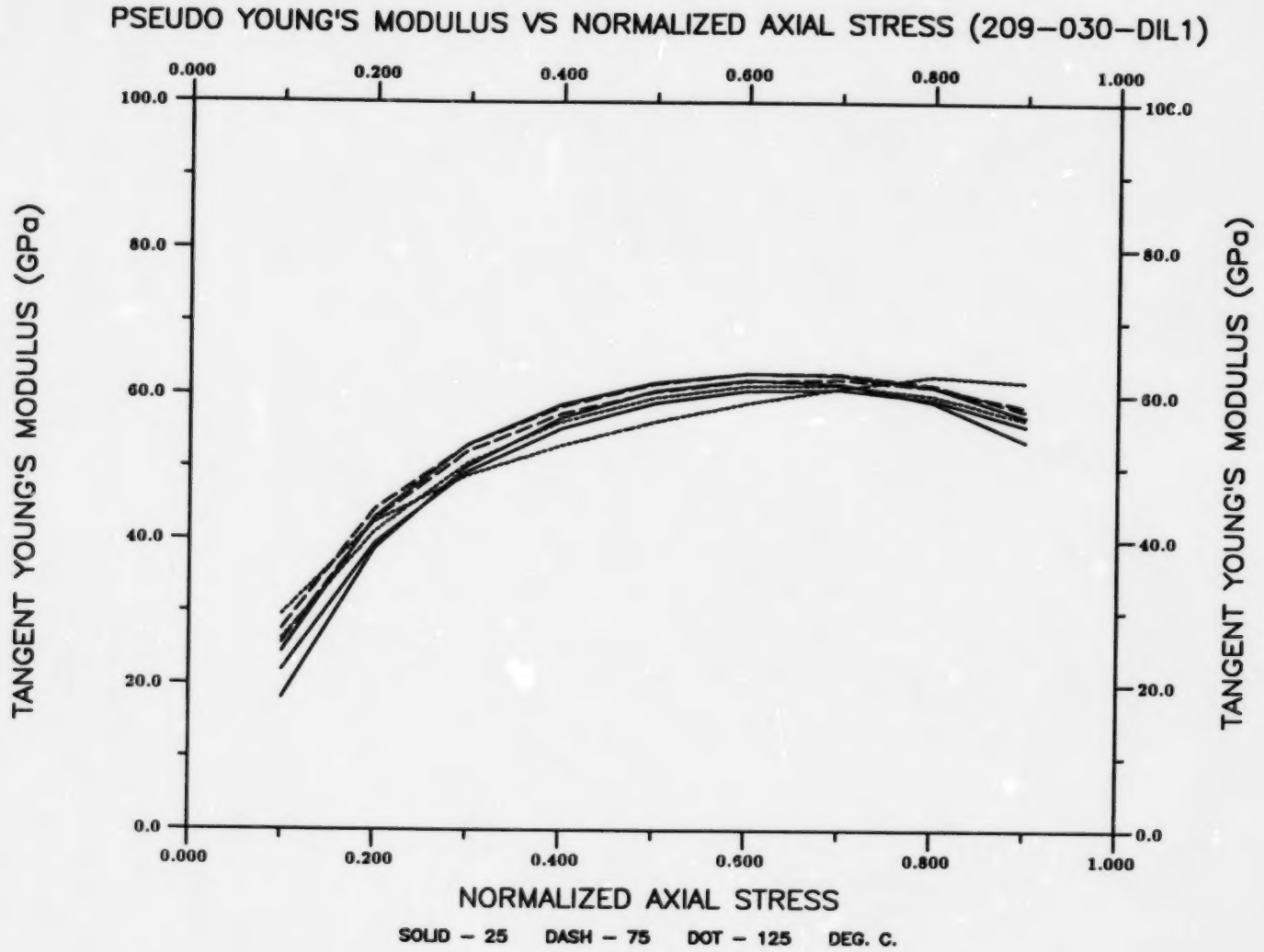

Figure 8. Plots of pseudo Young's modulus versus normalized axial stress for Borehole 209-030-DIL1.

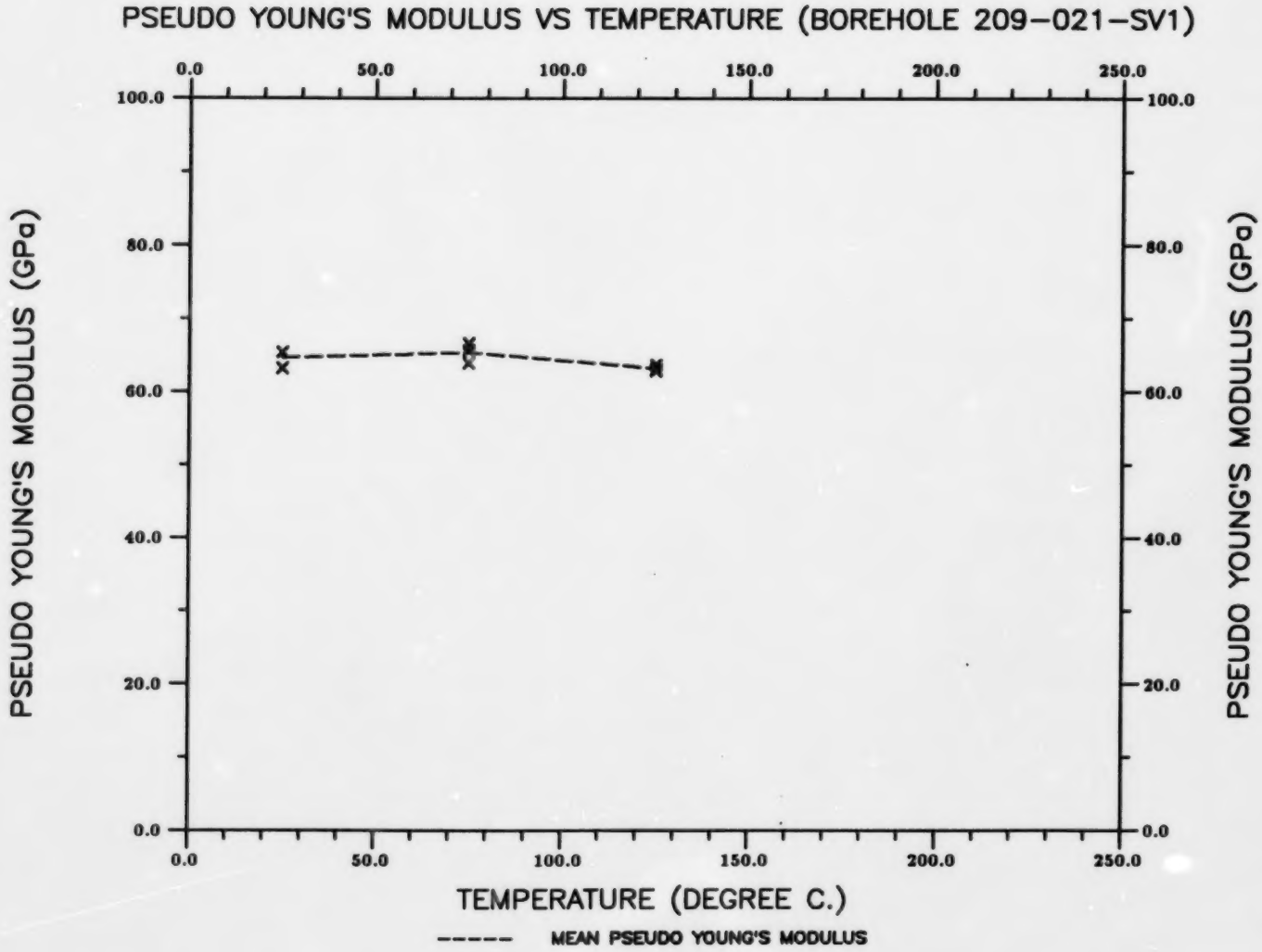

Figure 9. Plot of pseudo Young's modulus versus temperature for Borehole 209-021-SV1.

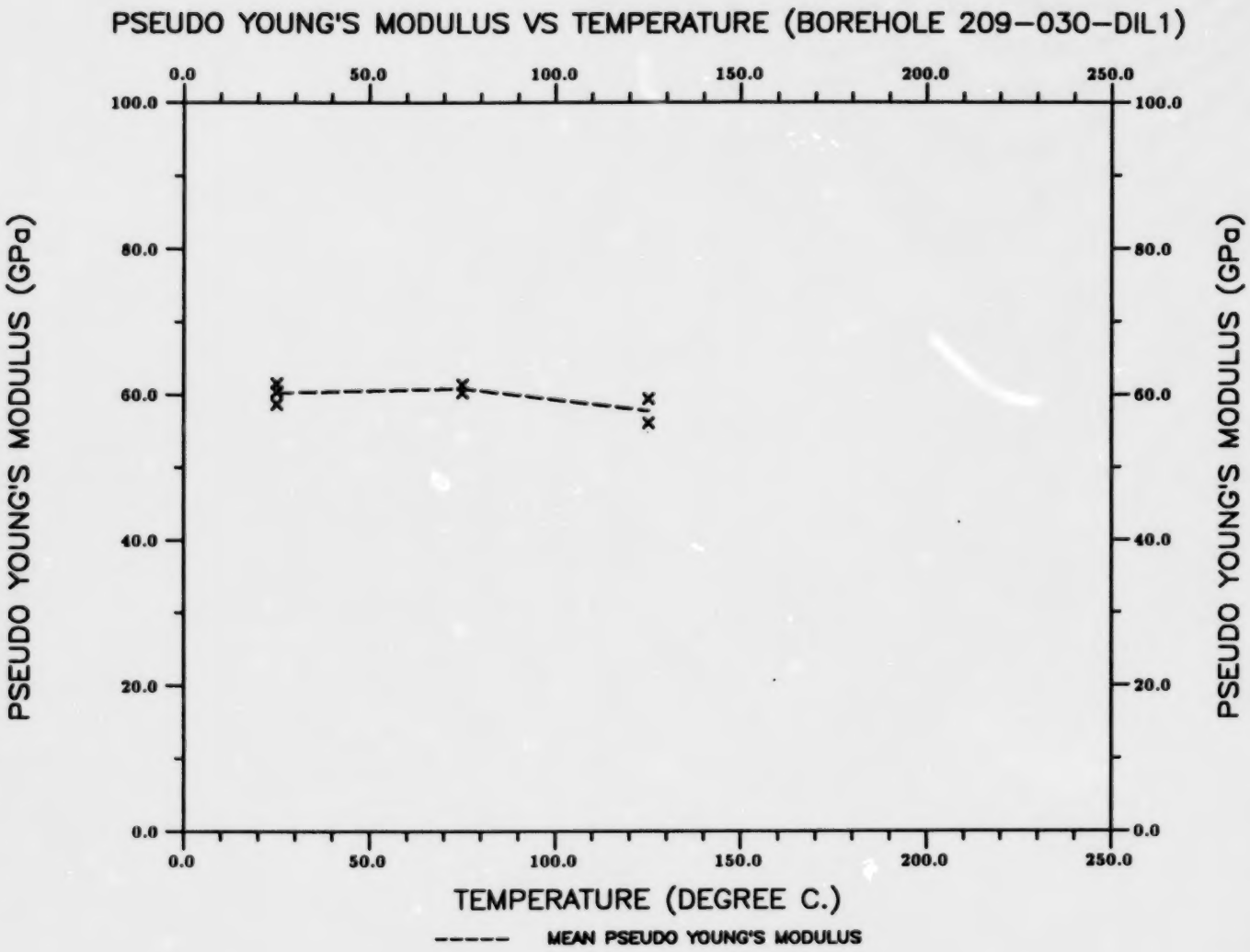

Figure 10. Plot of pseudo Young's modulus versus temperature for Borehole 209-030-DIL1.

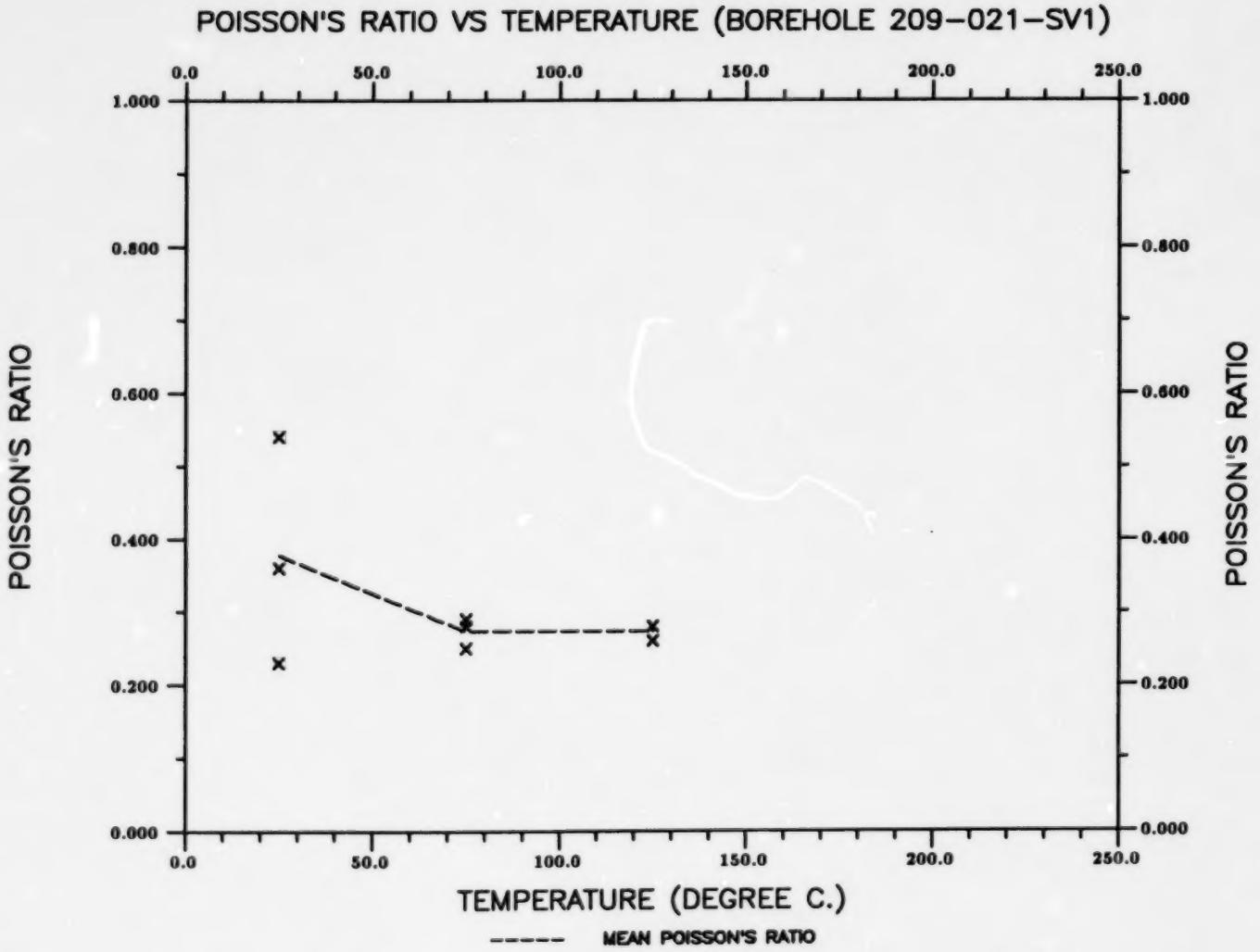

Figure 11. Plot of Poisson's ratio versus temperature for Borehole 209-021-SV1.

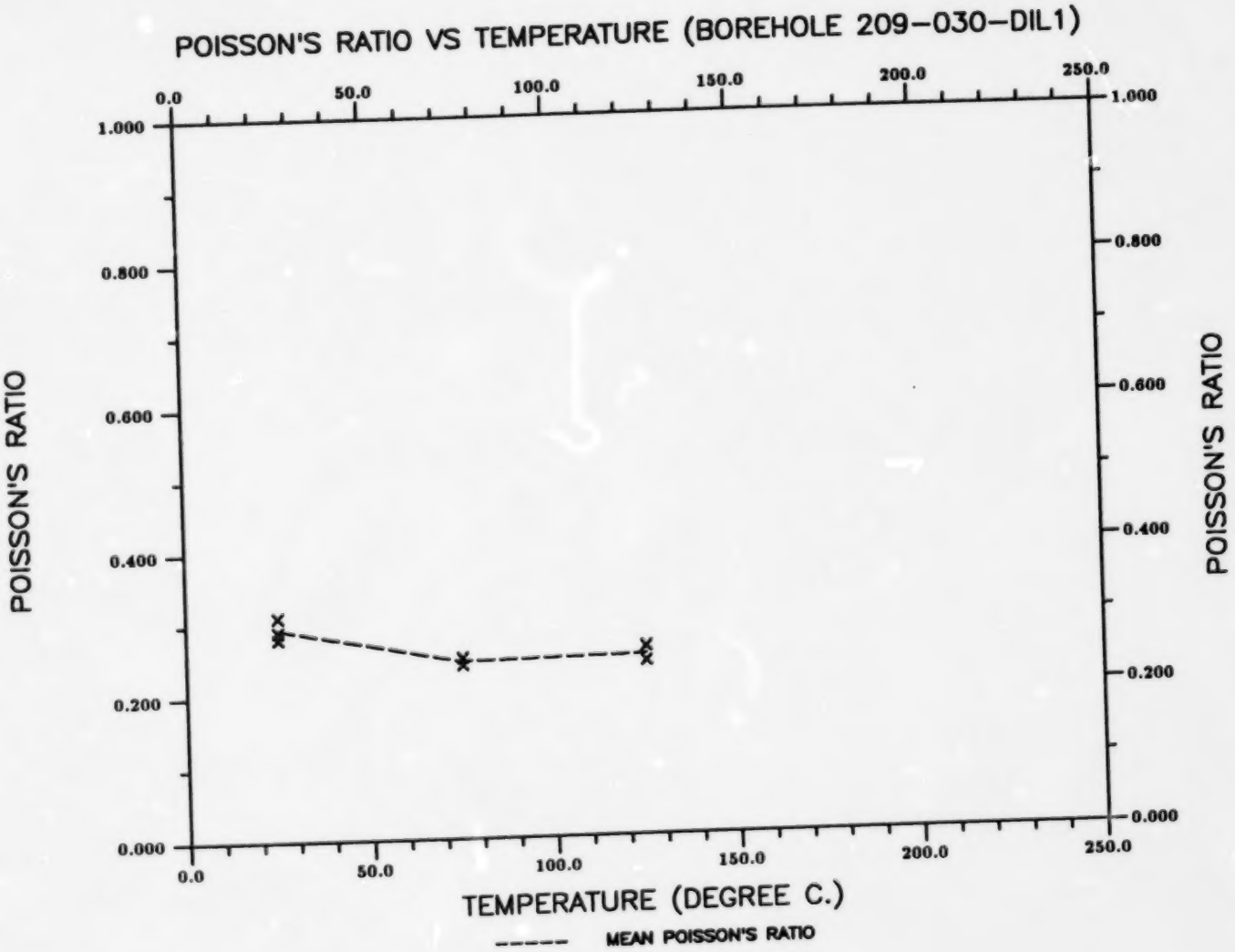

Figure 12. Plot of Poisson's ratio versus temperature for Borehole 209-030-DIL1.

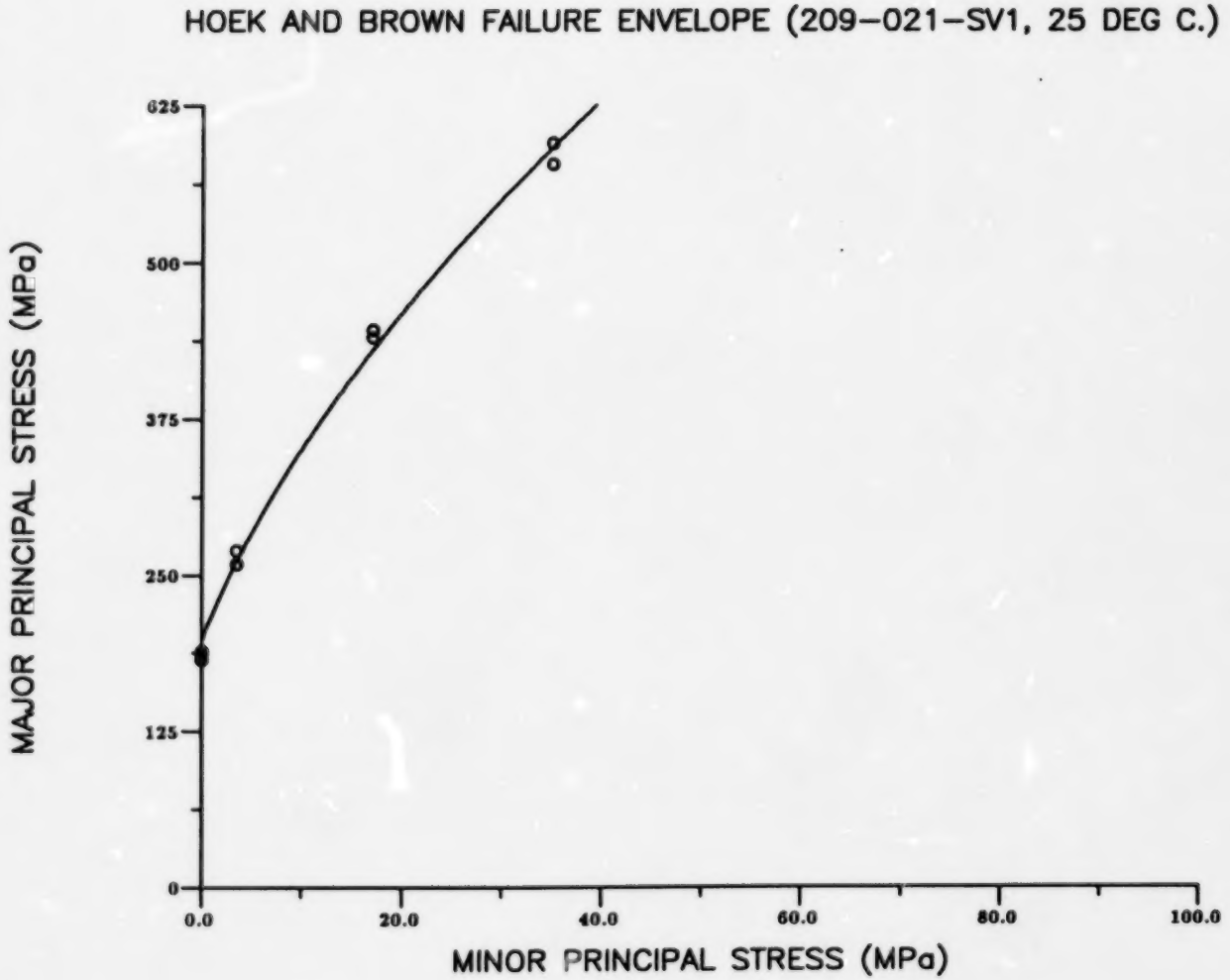

Figure 13. Hoek and Brown failure envelope for samples from Borehole 209-021-SV1 tested at 25° C.

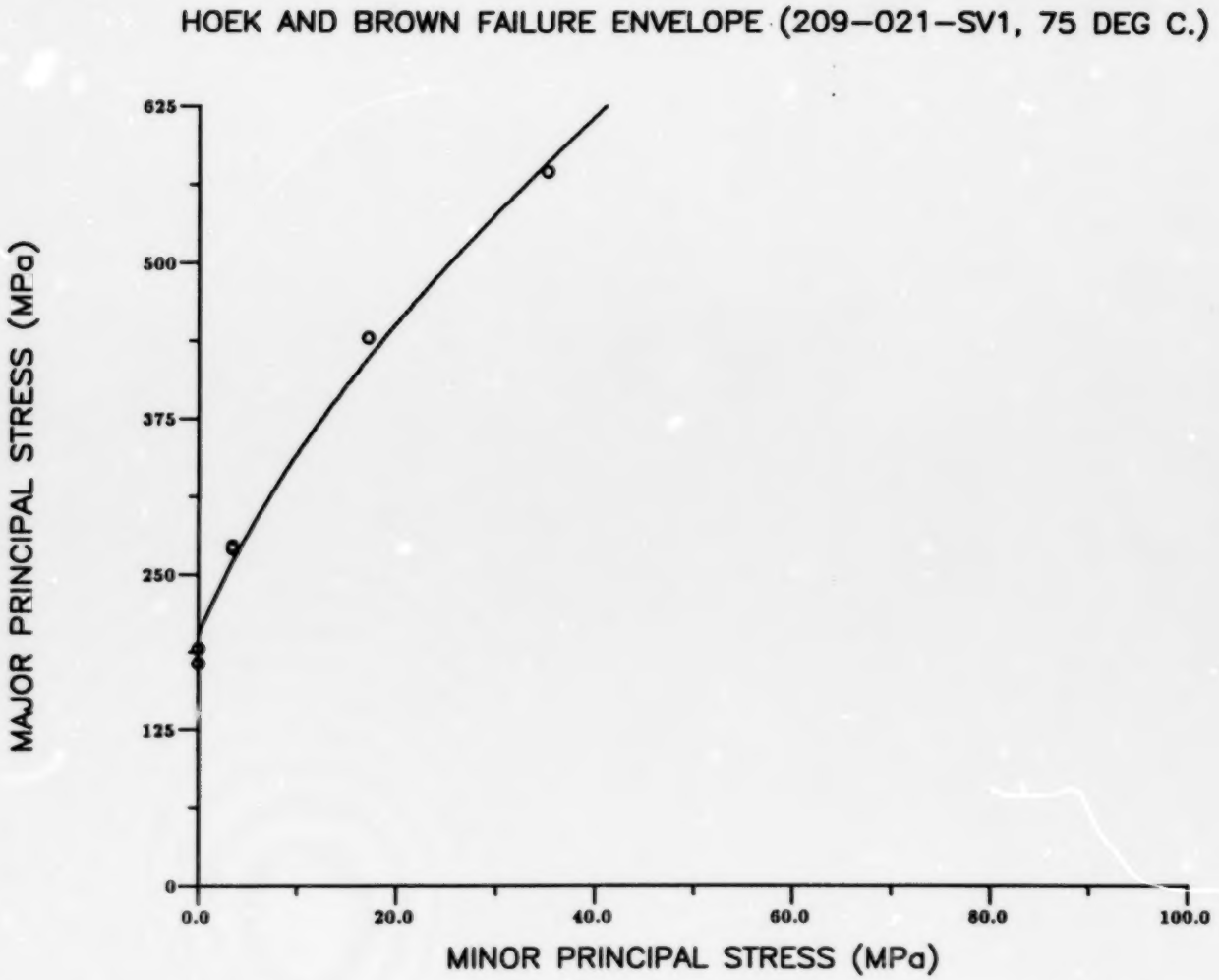

Figure 14. Hoek and Brown failure envelope for samples from Borehole 209-021-SV1 tested at 75° C.

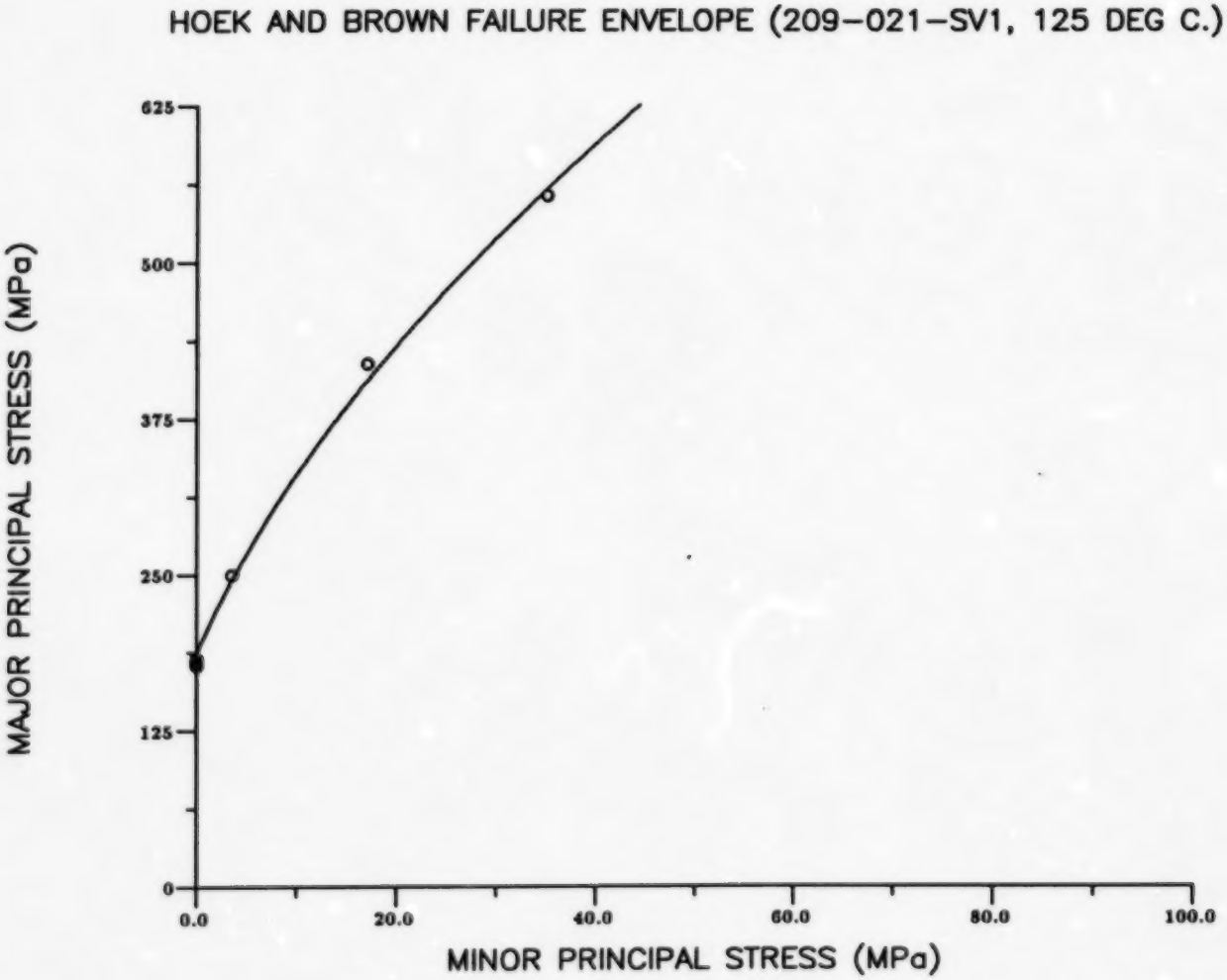

Figure 15. Hoek and Brown failure envelope for samples from Borehole 209-021-SV1 tested at 125° C.

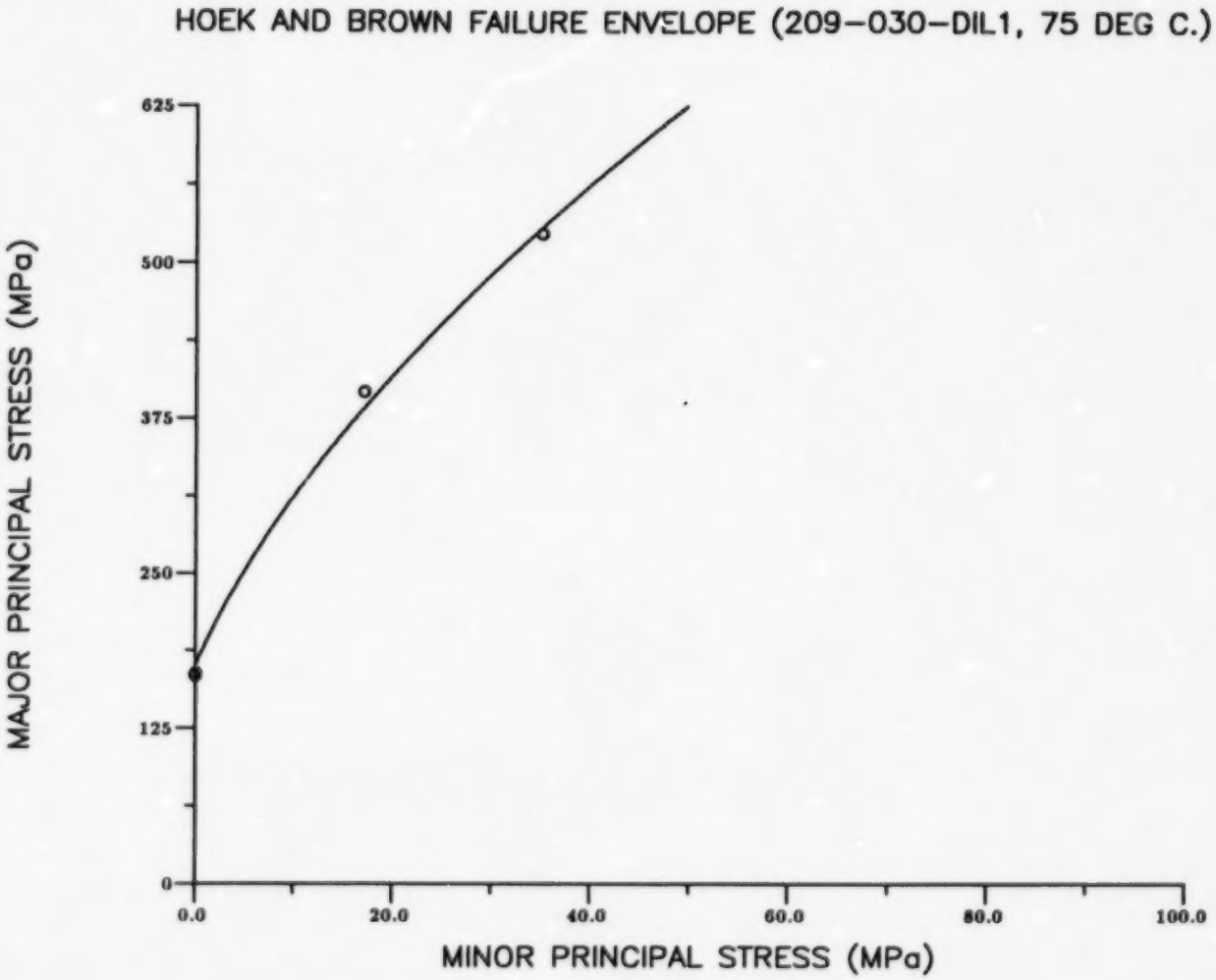

Figure 16. Hoek and Brown failure envelope for samples from Borehole 209-030-DIL1 tested at 75° C.

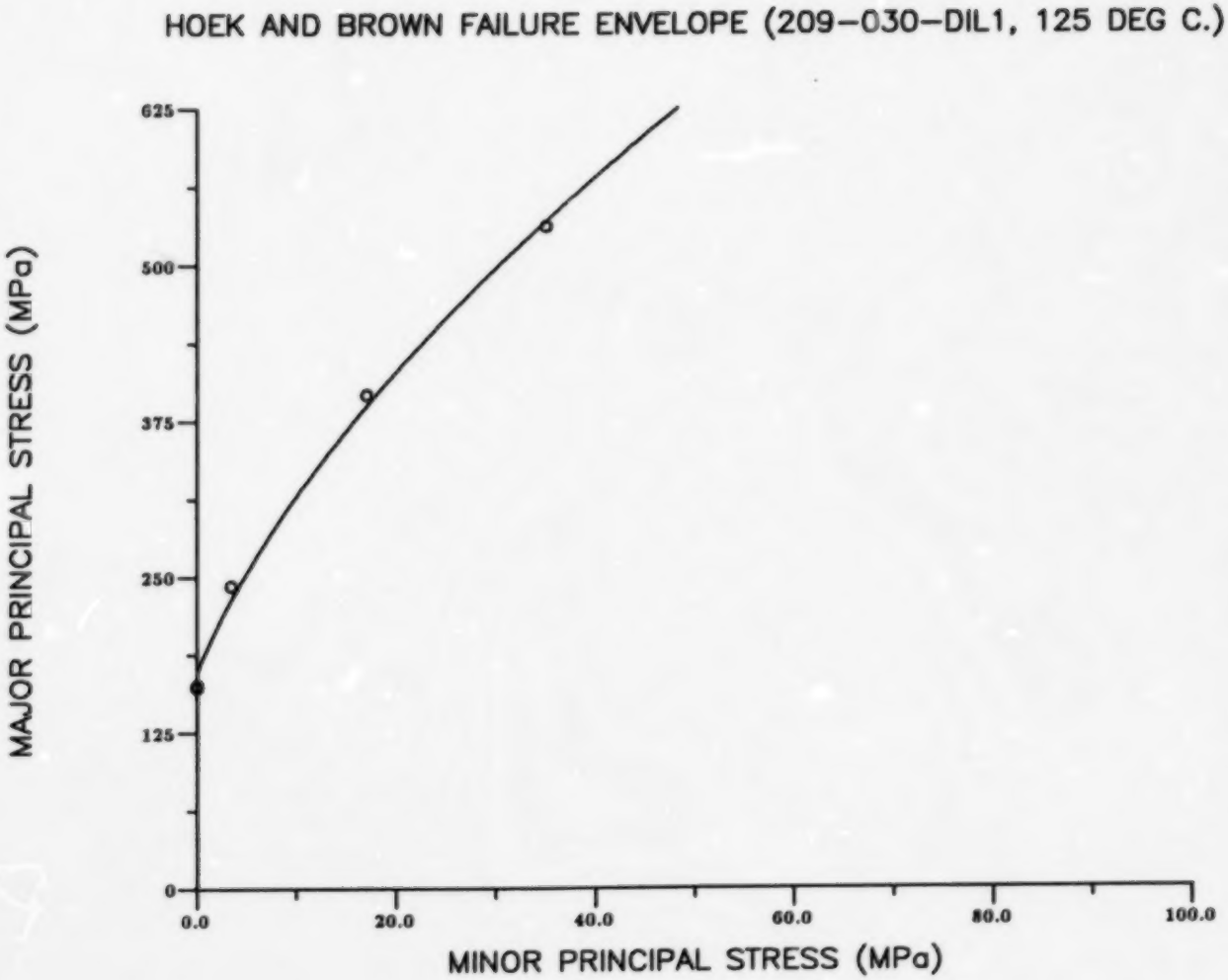

Figure 17. Hoek and Brown failure envelope for samples from Borehole 209-030-DIL1 tested at 125° C.

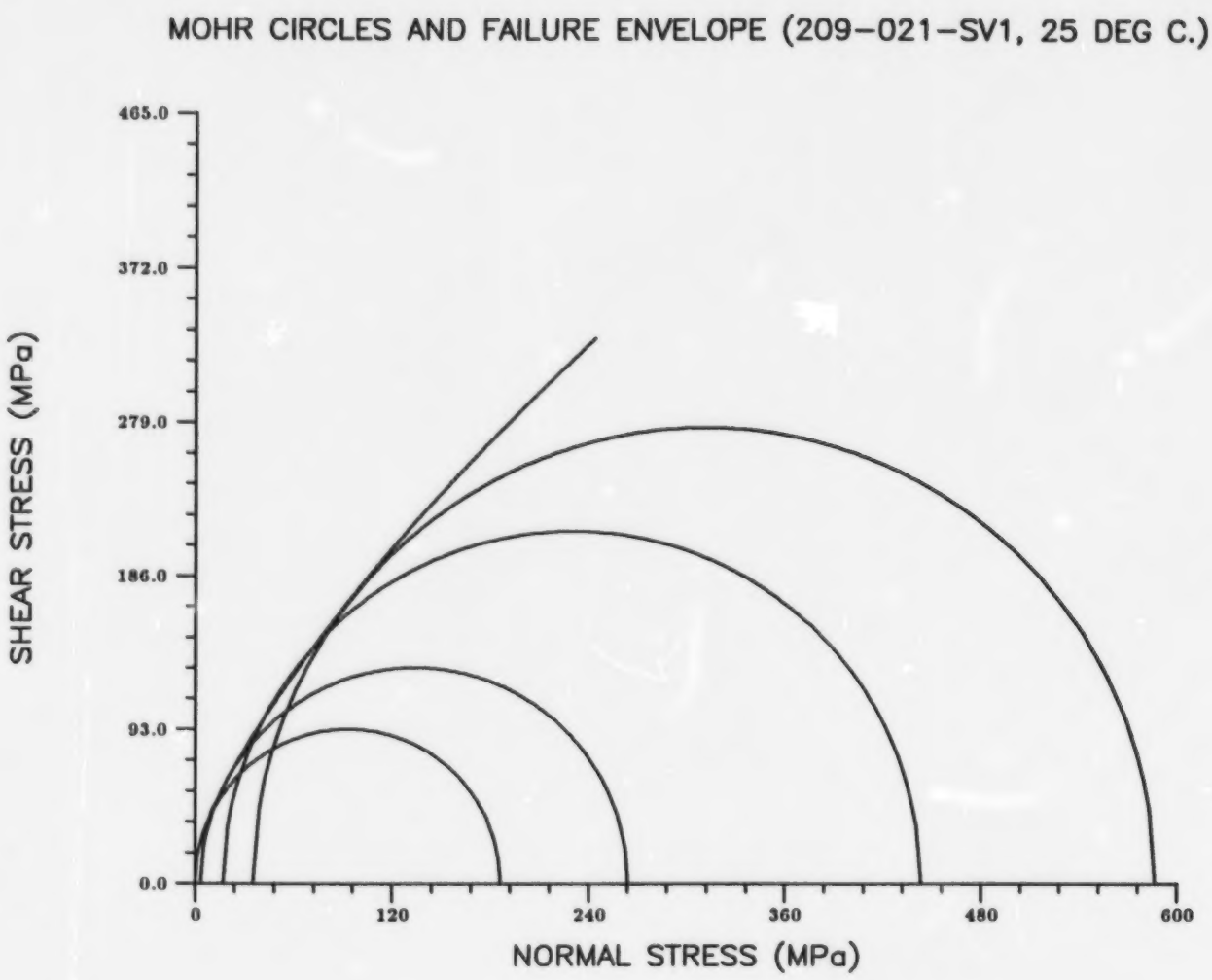

Figure 18. Mohr circles and failure envelope for samples from Borehole 209-021-SV1 tested at 25° C.

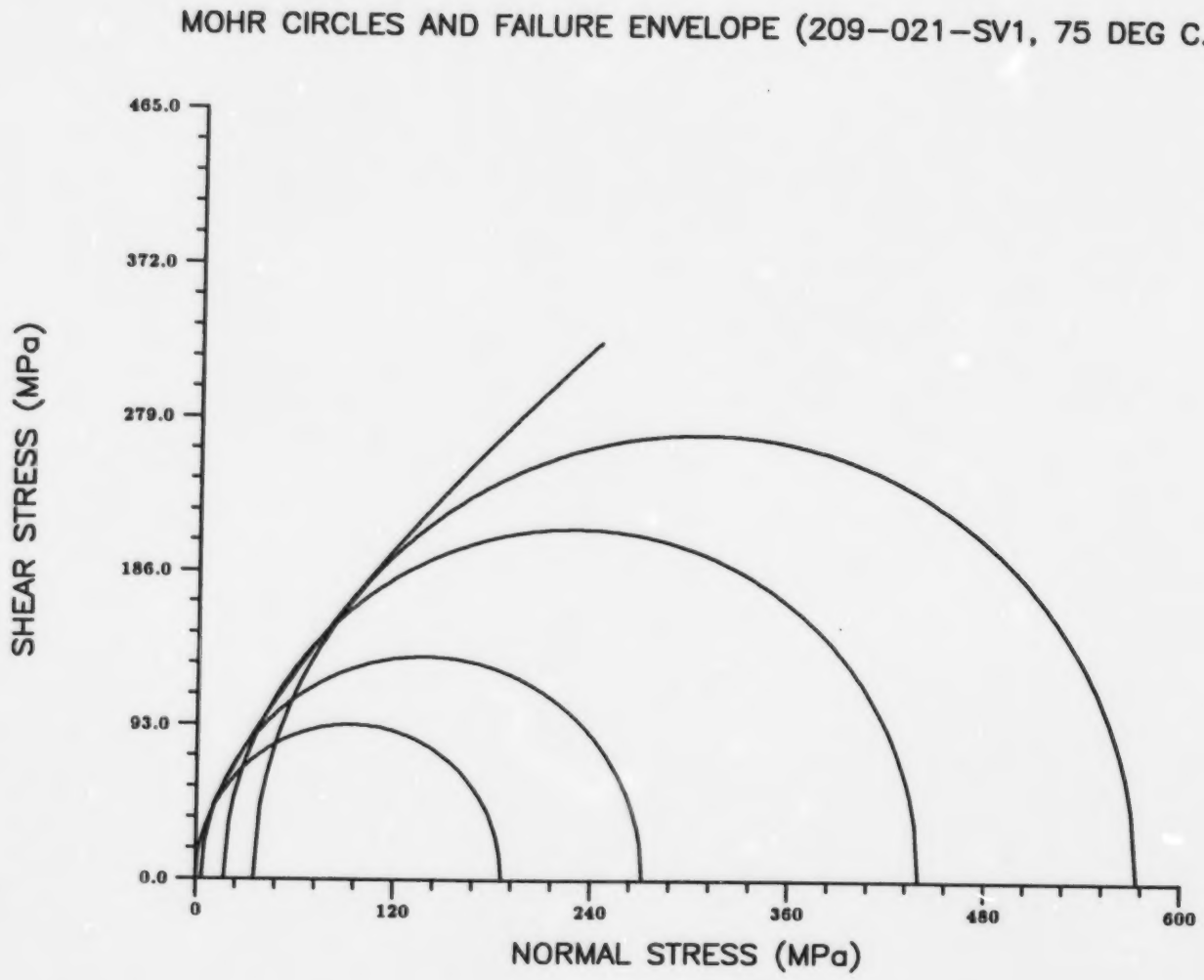

Figure 19. Mohr circles and failure envelope for samples from Borehole 209-021-SV1 tested at 75° C.

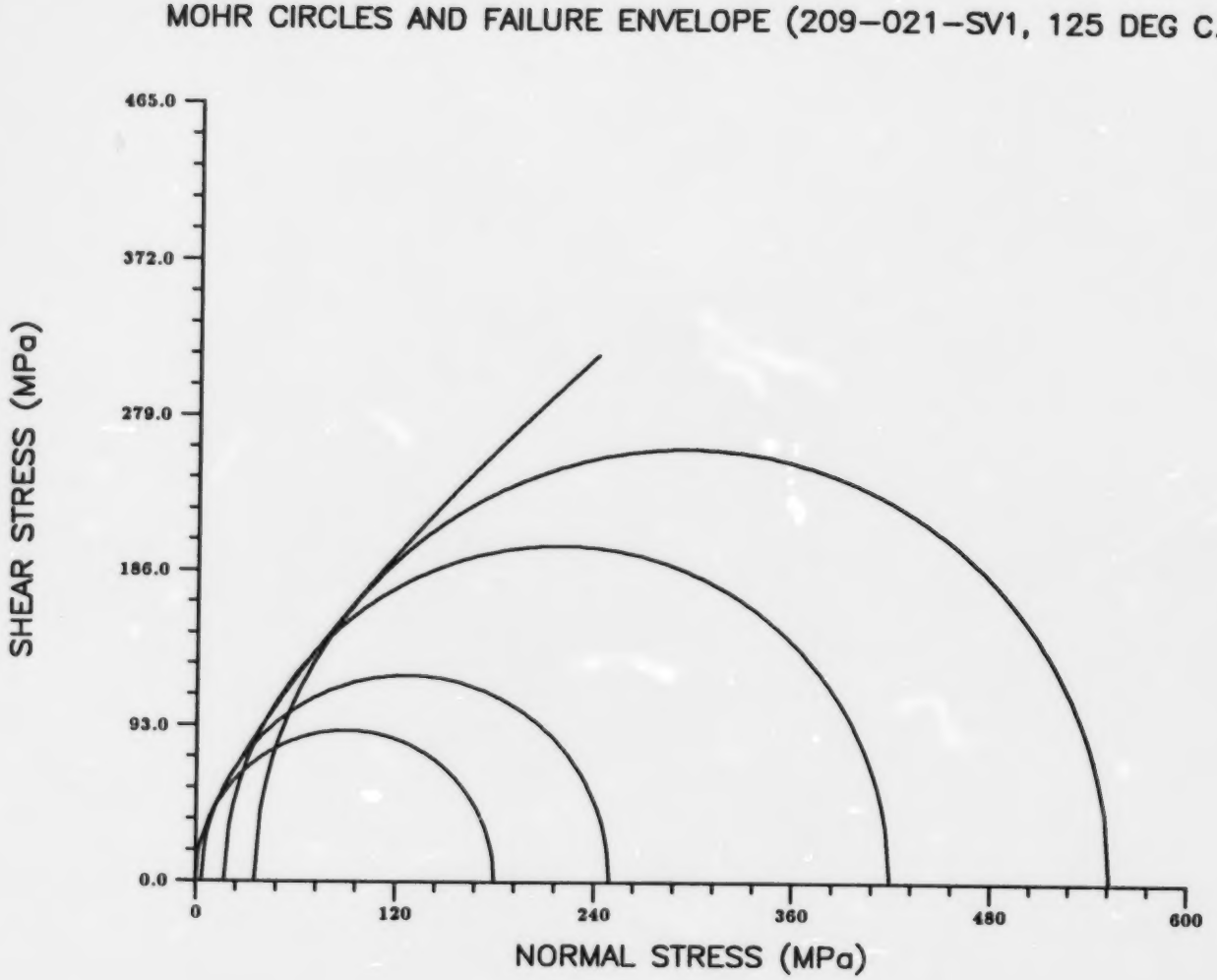

Figure 20. Mohr circles and failure envelope for samples from Borehole 209-021-SV1 tested at 125° C.

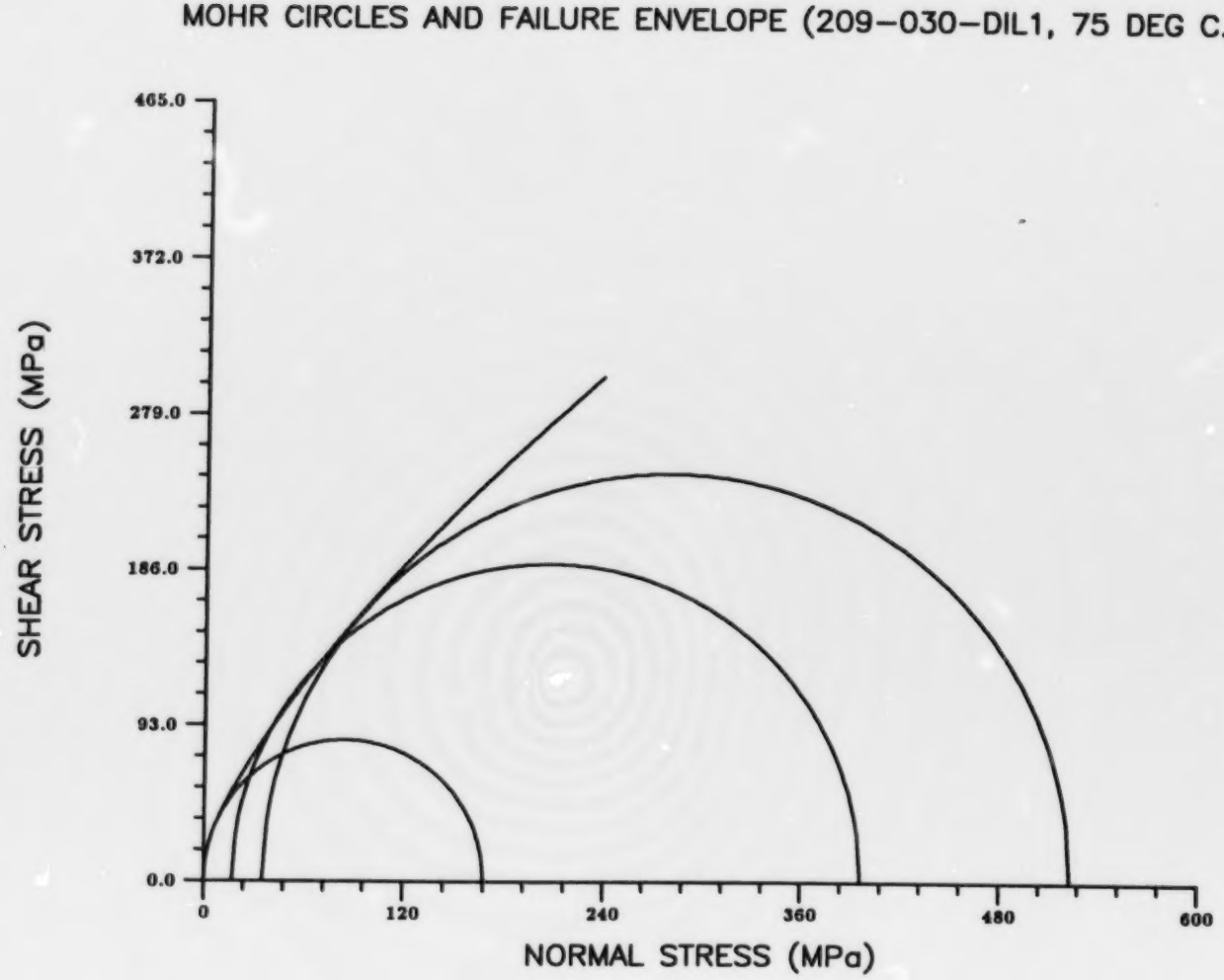

Figure 21. Mohr circles and failure envelope for samples from Borehole 209-030-DIL1 tested at 75° C.

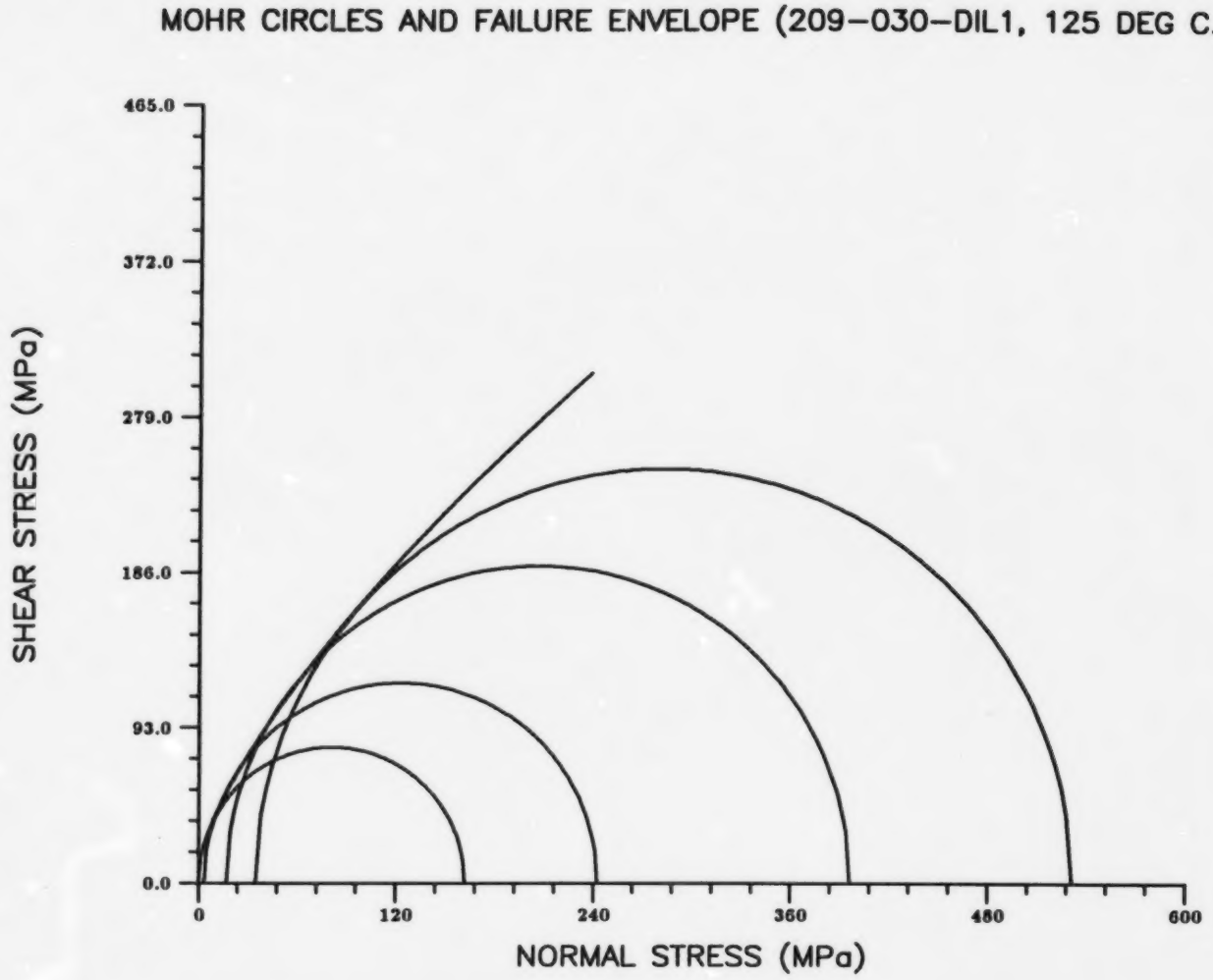

Figure 22. Mohr circles and failure envelope for samples from Borehole 209-030-DIL1 tested at 125° C.

Appendix A

Stress-strain curves for specimens from Borehole 209-021-SV1

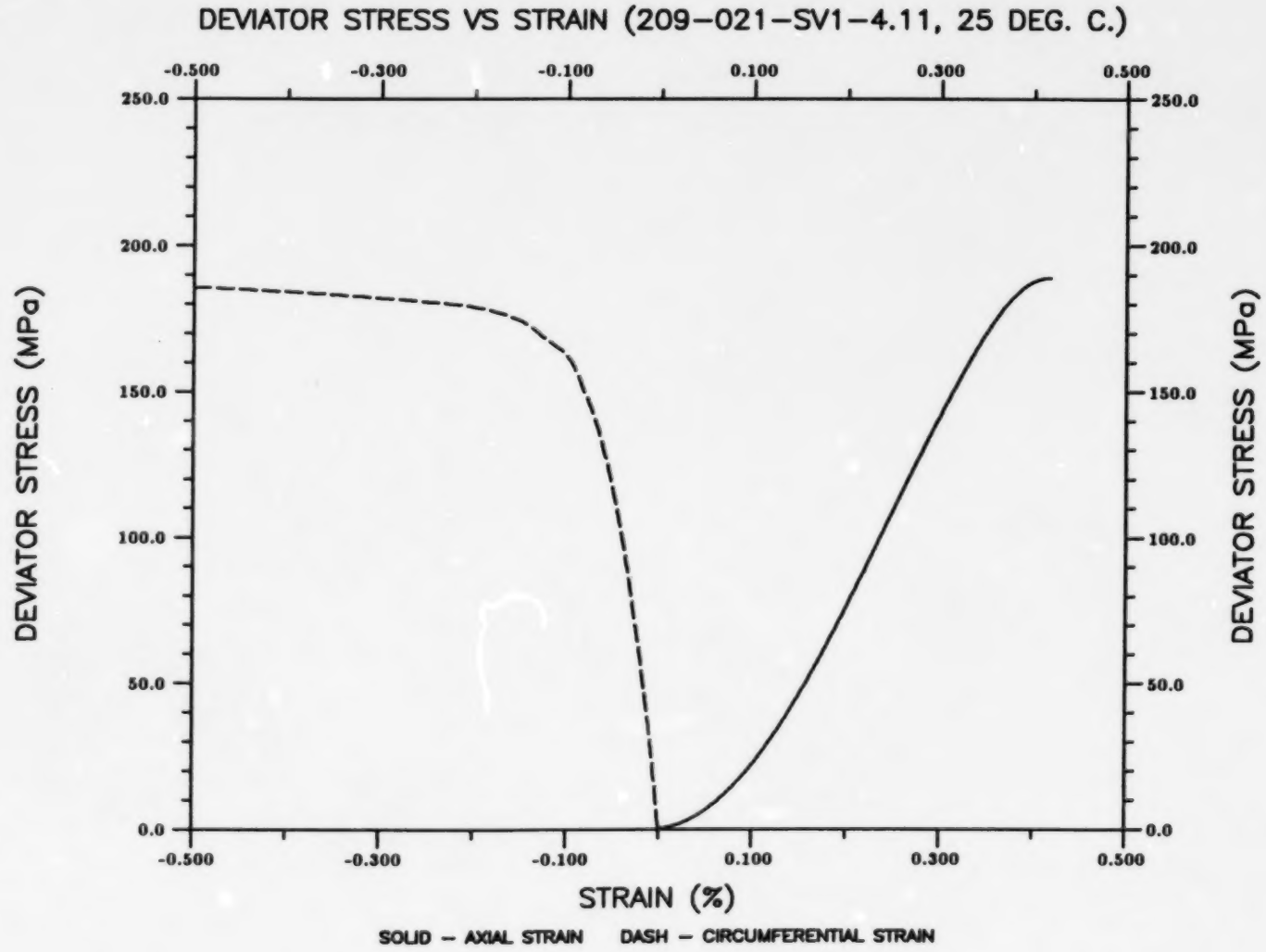

Figure A1. Stress-strain curves for Specimen 209-021-SV1-4.11 tested at 25° C.

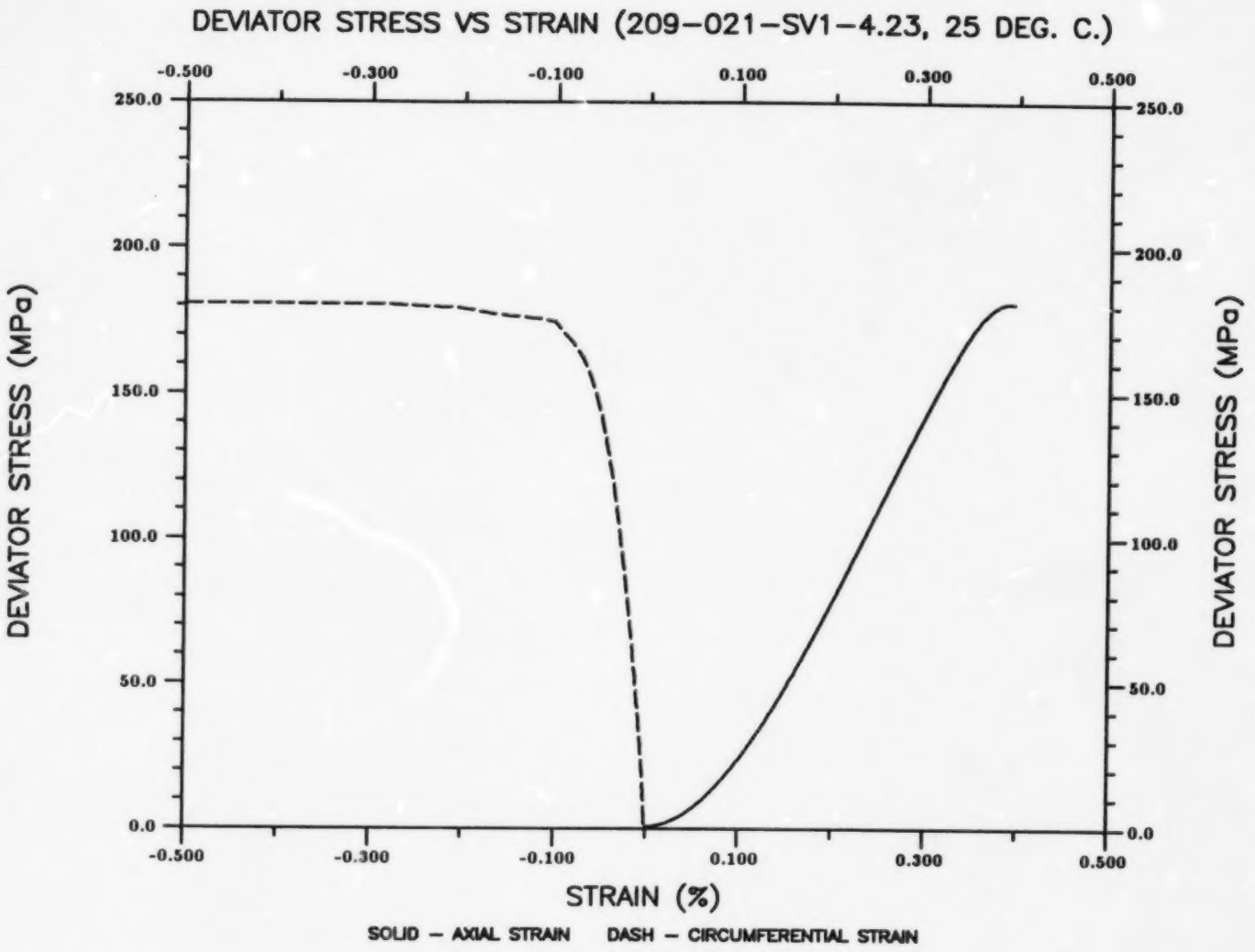

Figure A2. Stress-strain curves for Specimen 209-021-SV1-4.23 tested at 25° C.

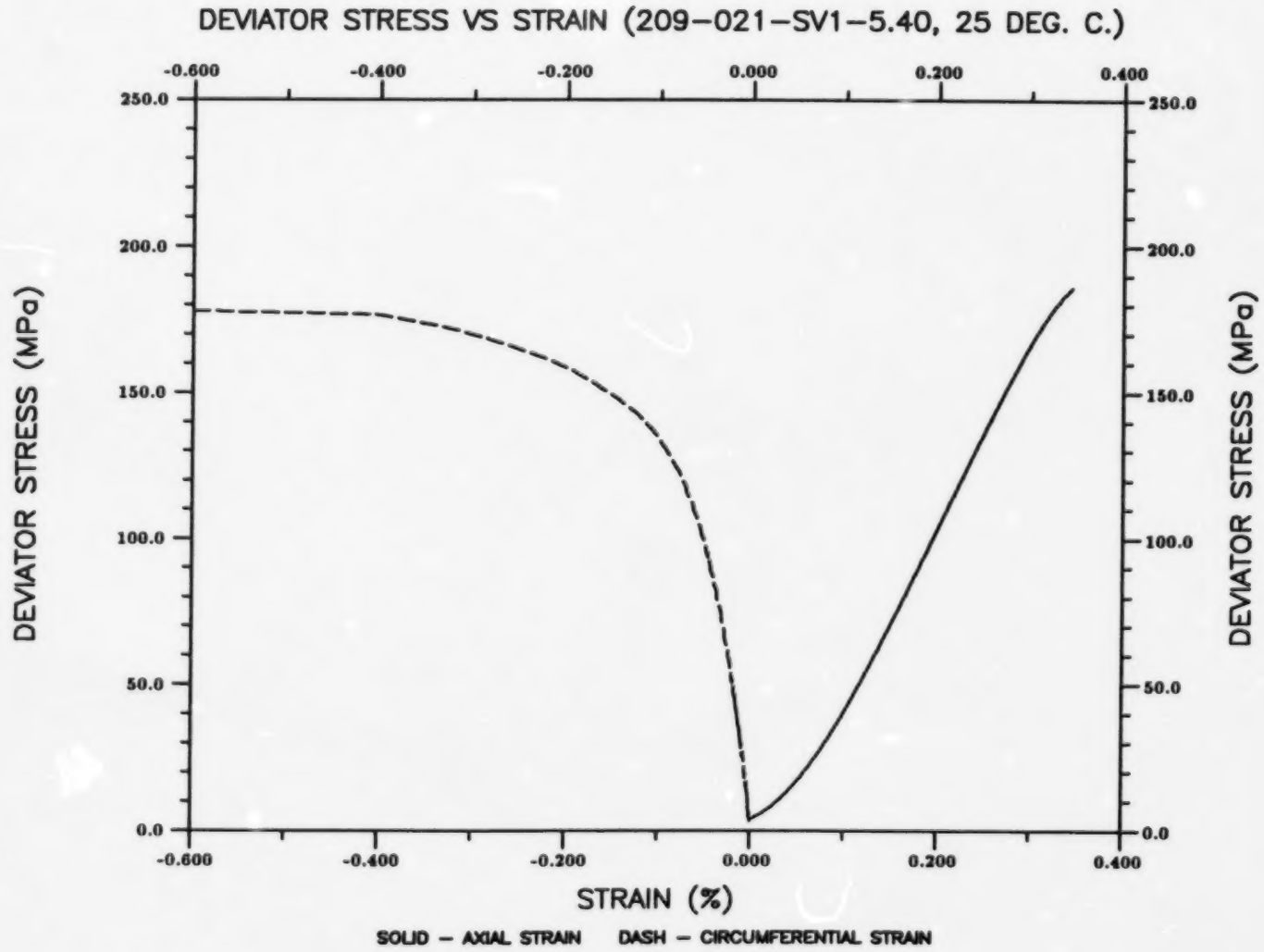

Figure A3. Stress-strain curves for Specimen 209-021-SV1-5.40 tested at 25° C.

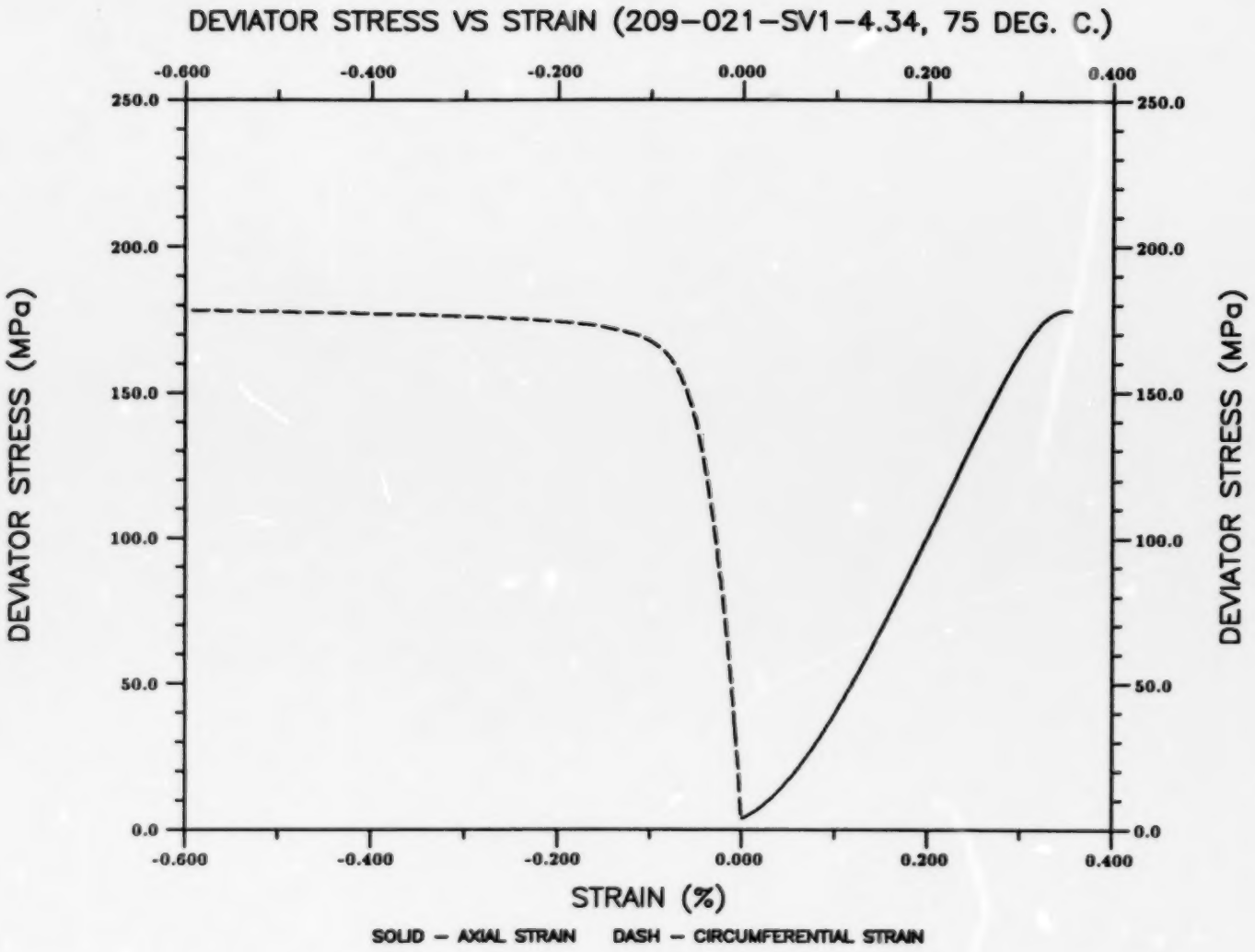

Figure A4. Stress-strain curves for Specimen 209-021-SV1-4.34 tested at 75° C.

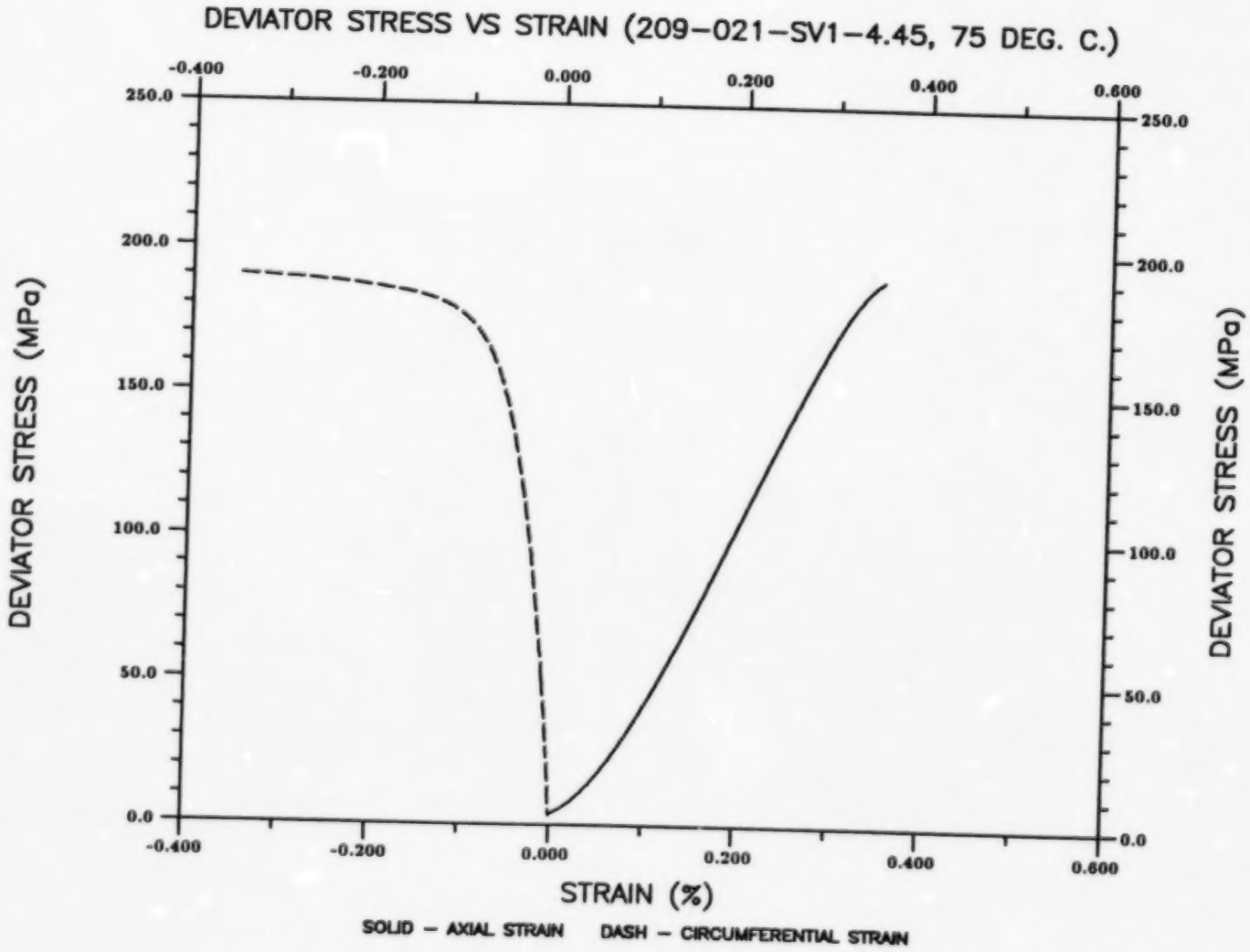

Figure A5. Stress-strain curves for Specimen 209-021-SV1-4.45 tested at 75° C.

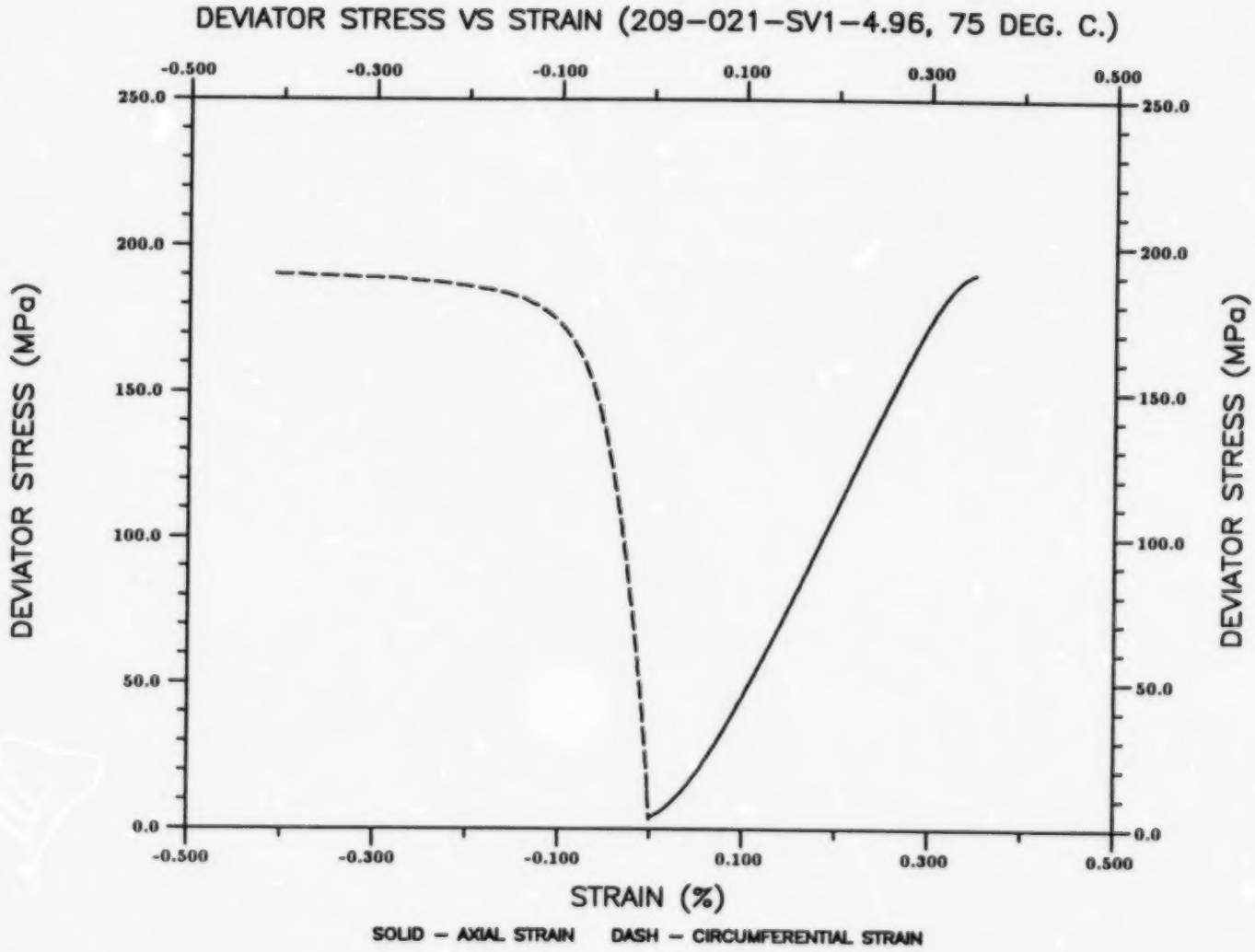

Figure A6. Stress-strain curves for Specimen 209-021-SV1-4.96 tested at 75° C.

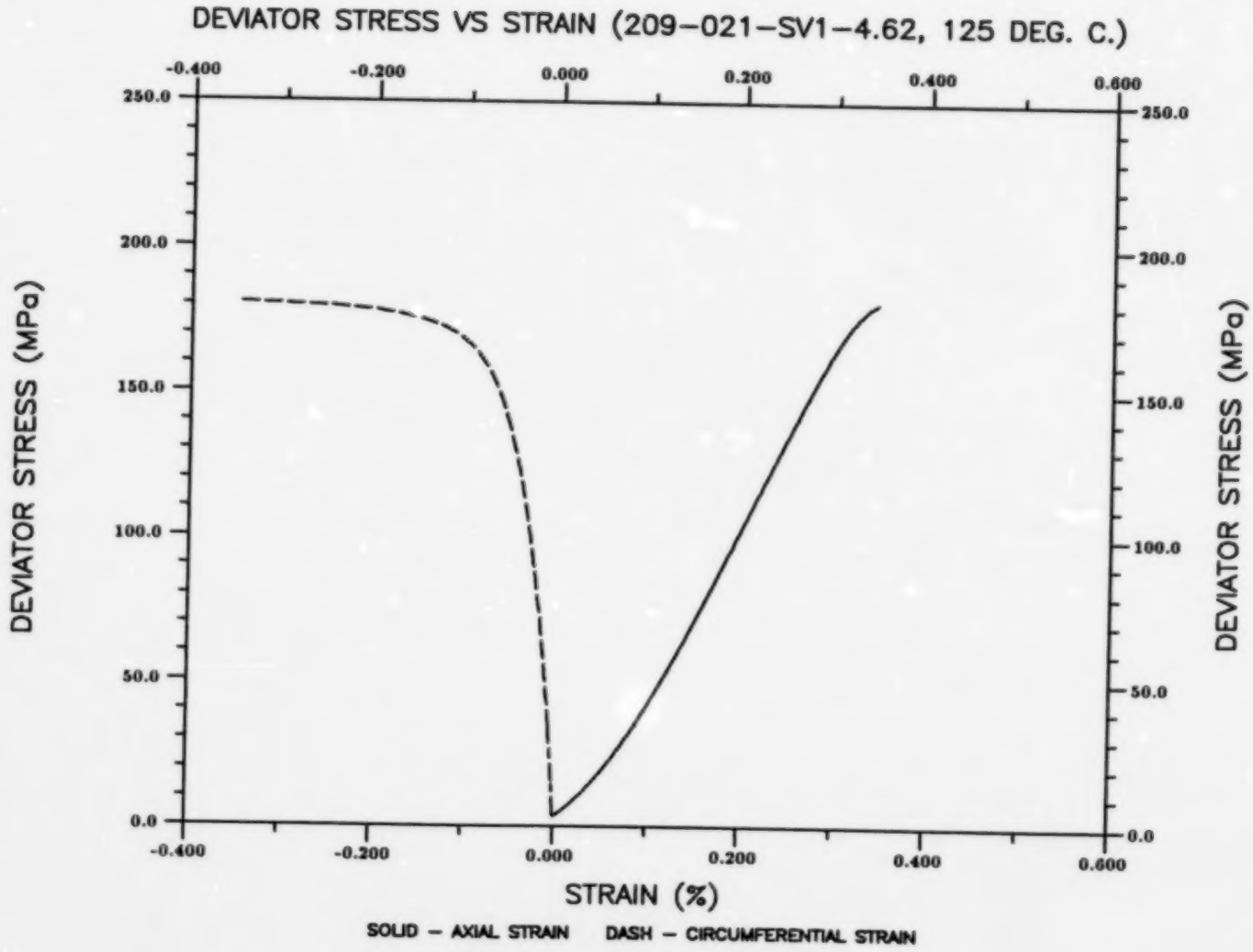

Figure A7. Stress-strain curves for Specimen 209-021-SV1-4.62 tested at 125° C.

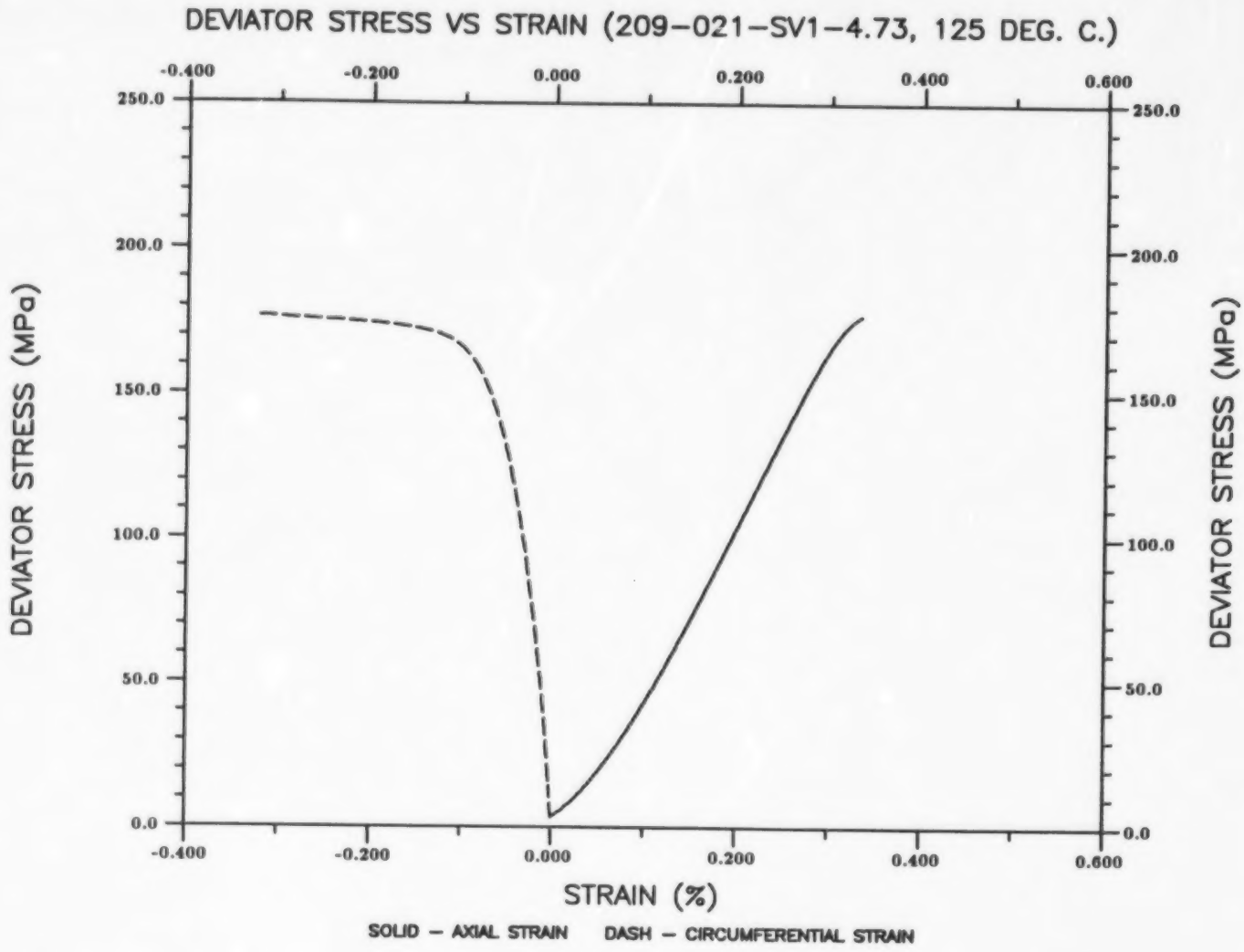

Figure A8. Stress-strain curves for Specimen 209-021-SV1-4.73 tested at 125° C.

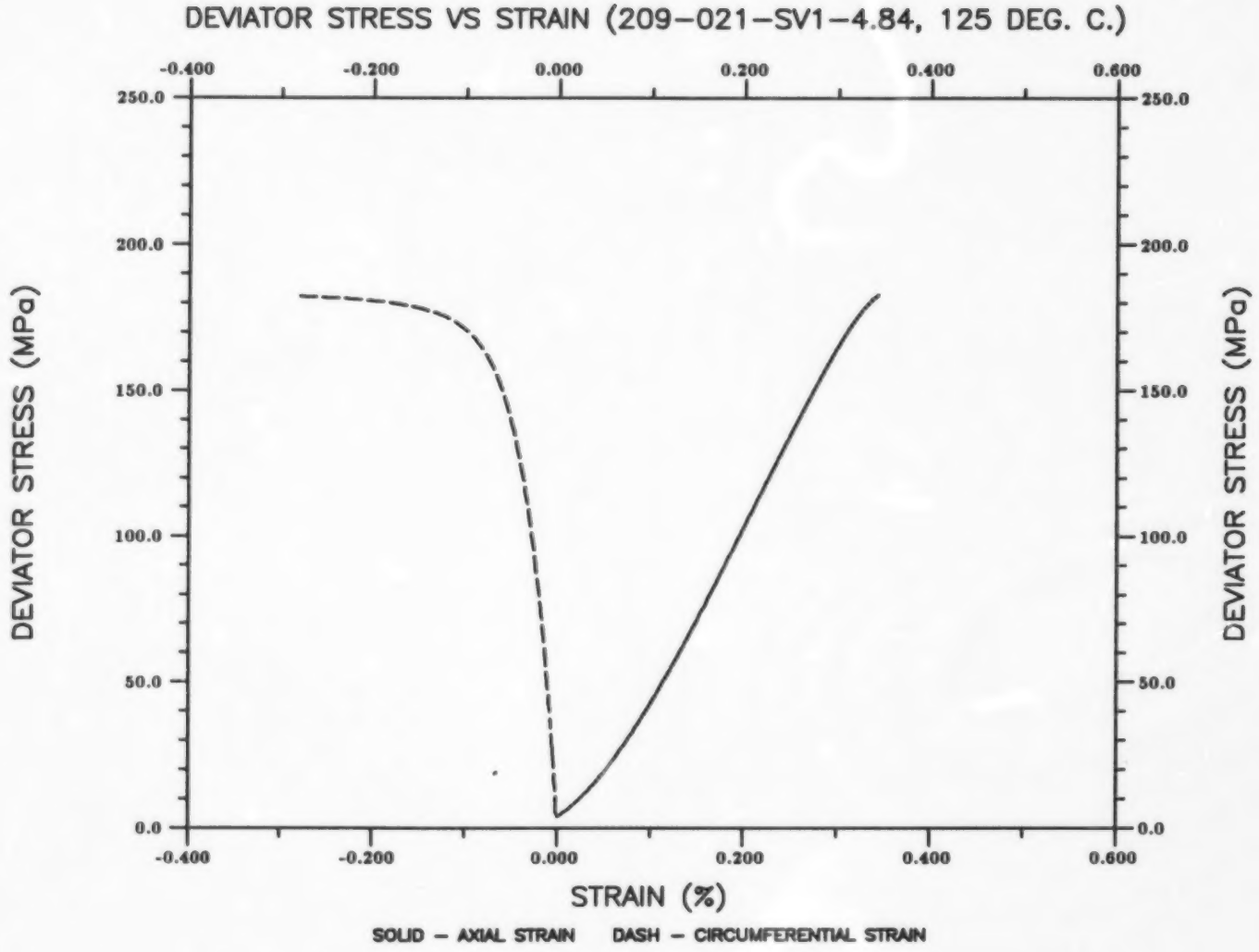

Figure A9. Stress-strain curves for Specimen 209-021-SV1-4.84 tested at 125° C.

Appendix B

Stress-strain curves for specimens from Borehole 209-030-DIL1

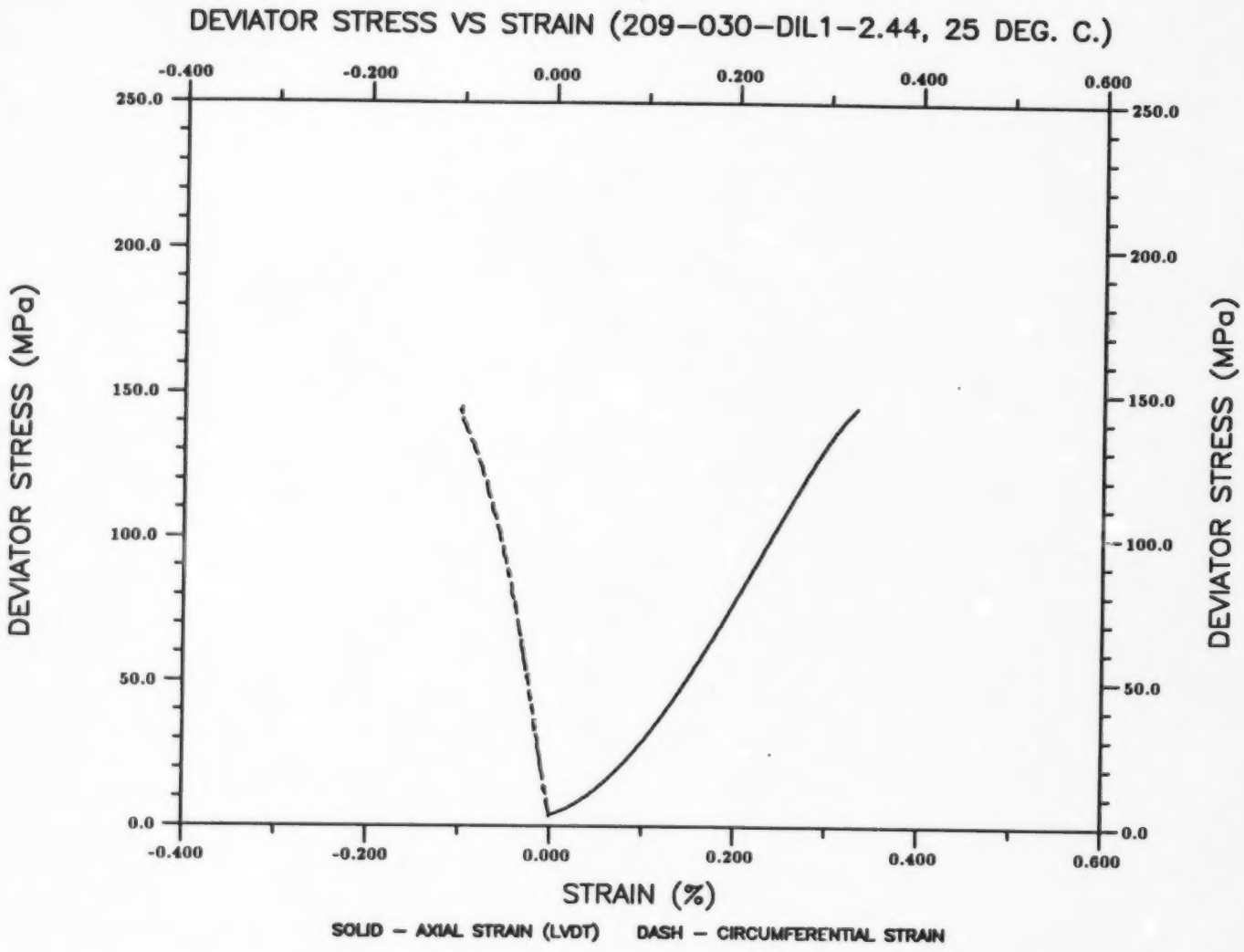

Figure B1. Stress-strain curves for Specimen 209-030-DIL1-2.44 tested at 25° C.

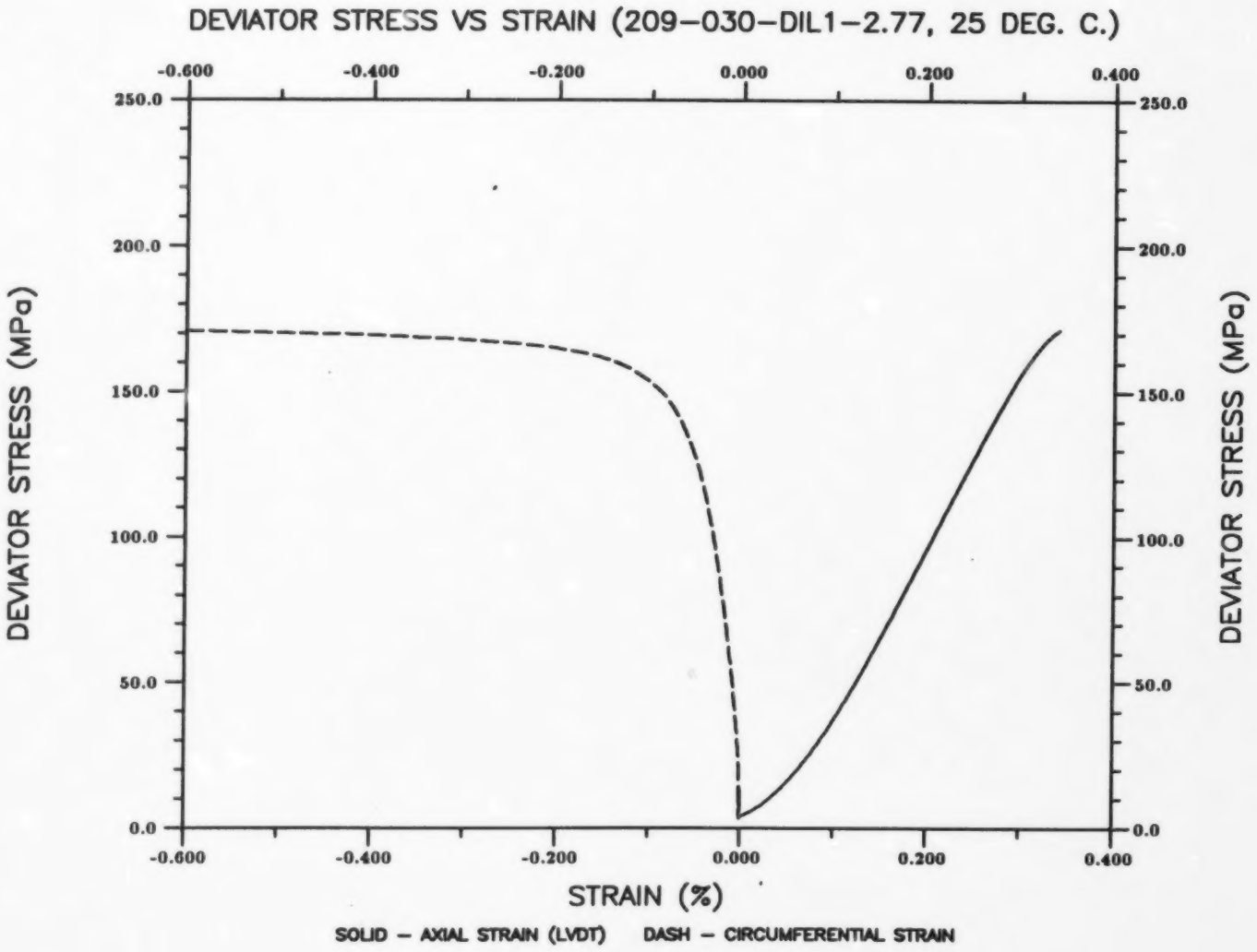

Figure B2. Stress-strain curves for Specimen 209-030-DIL1-2.77 tested at 25° C.

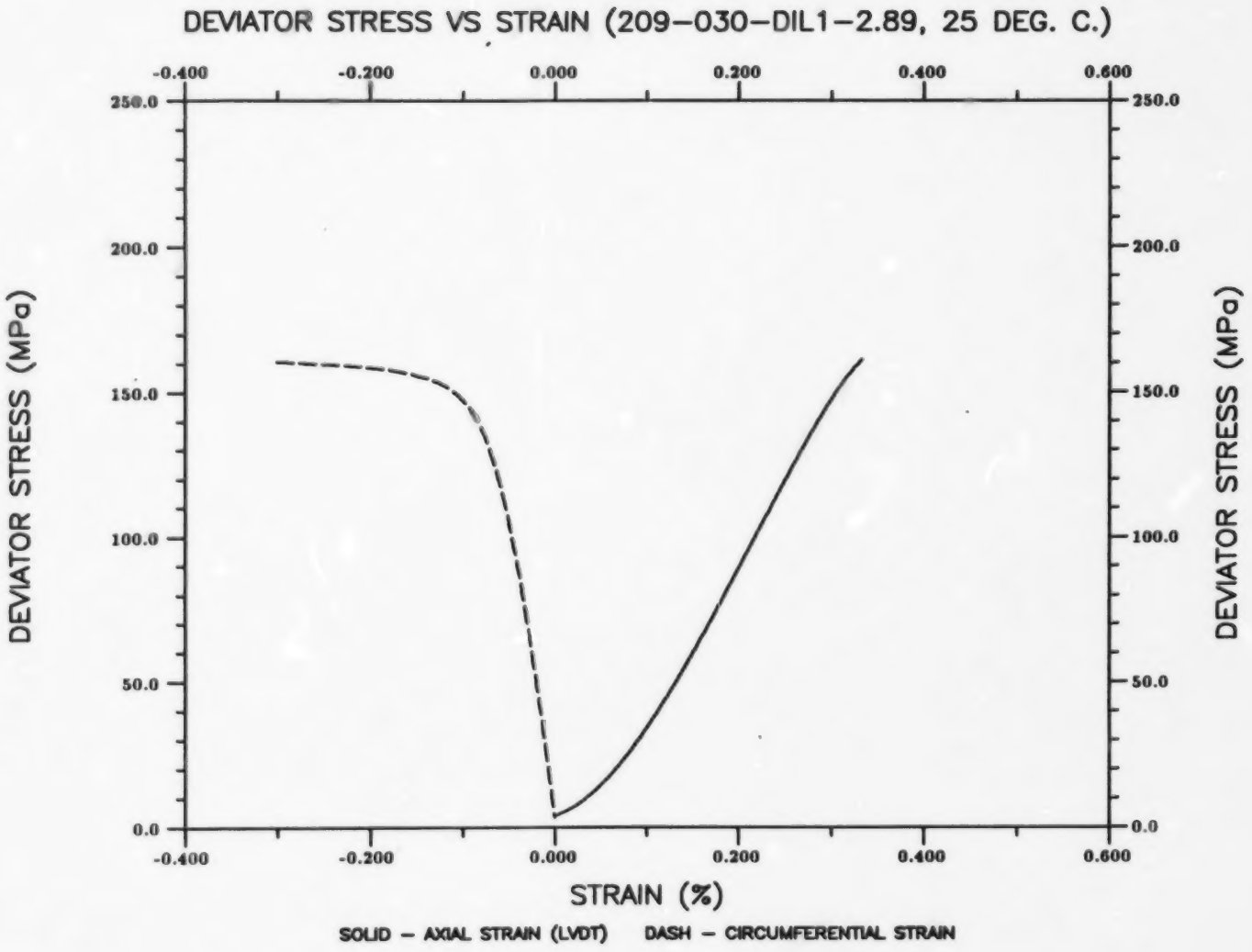

Figure B3. Stress-strain curves for Specimen 209-030-DIL1-2.89 tested at 25° C.

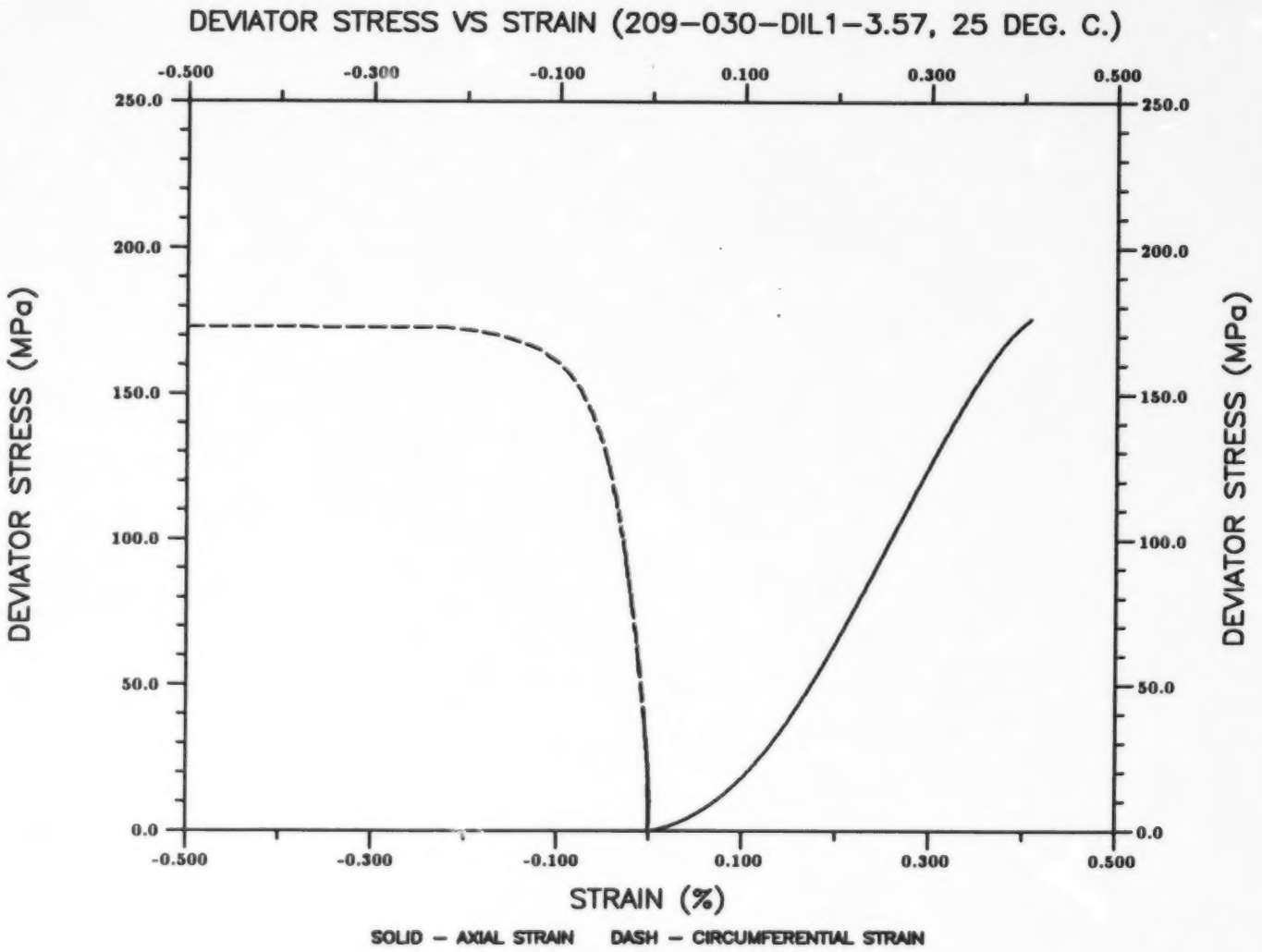

Figure B4. Stress-strain curves for Specimen 209-030-DIL1-3.57 tested at 25° C.

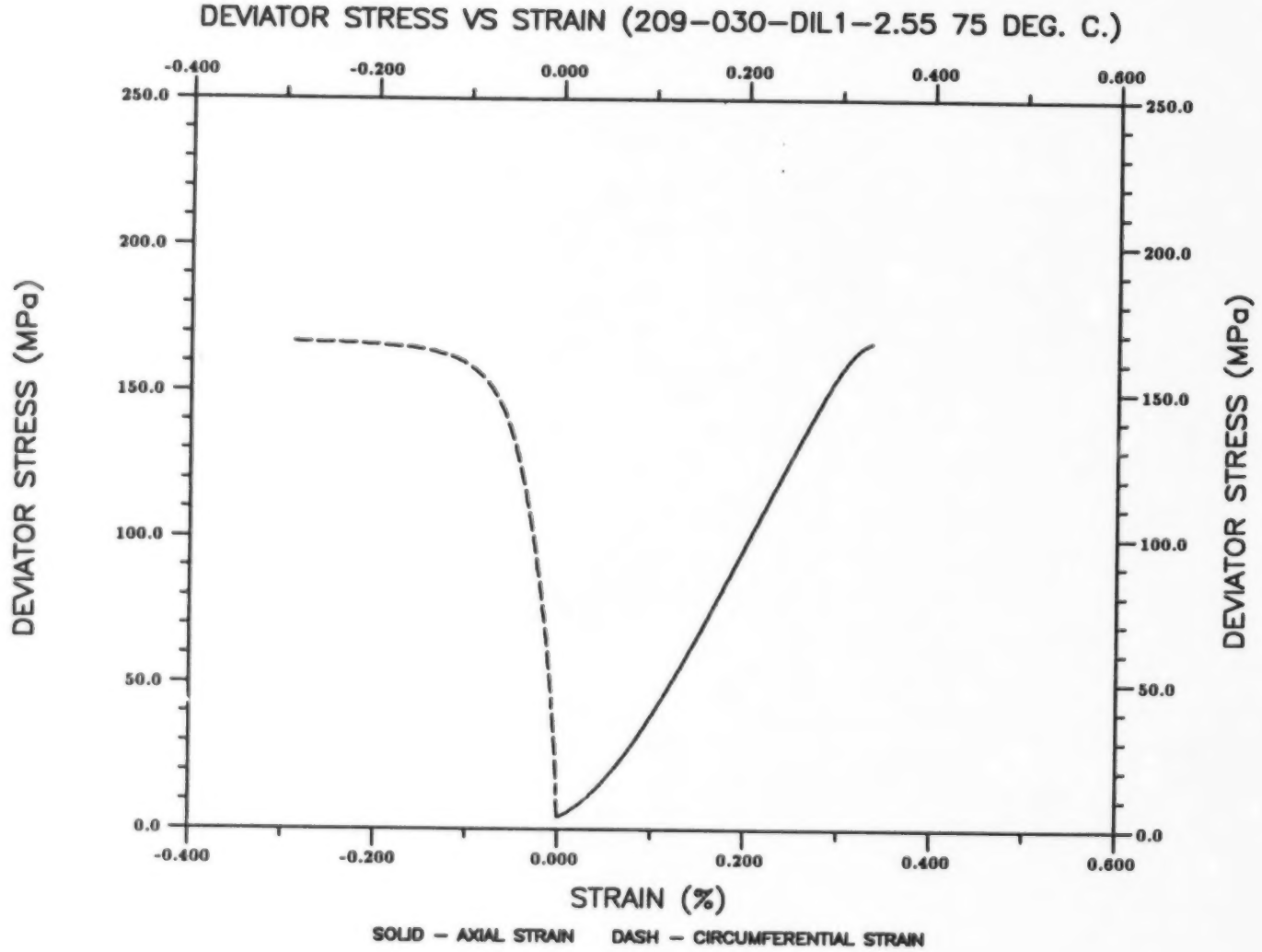

Figure B5. Stress-strain curves for Specimen 209-030-DIL1-2.55 tested at 75° C.

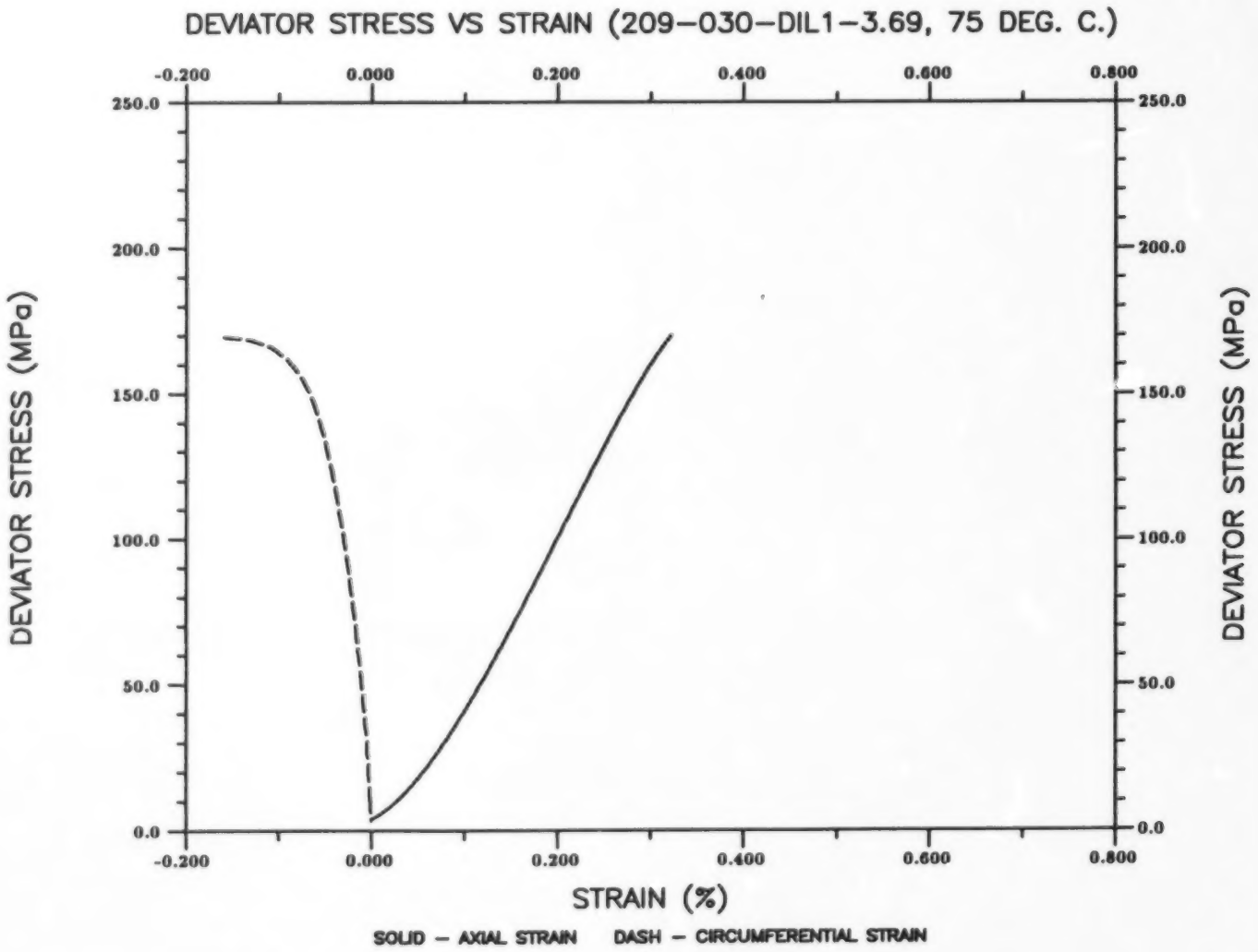

Figure B6. Stress-strain curves for Specimen 209-030-DIL1-3.69 tested at 75° C.

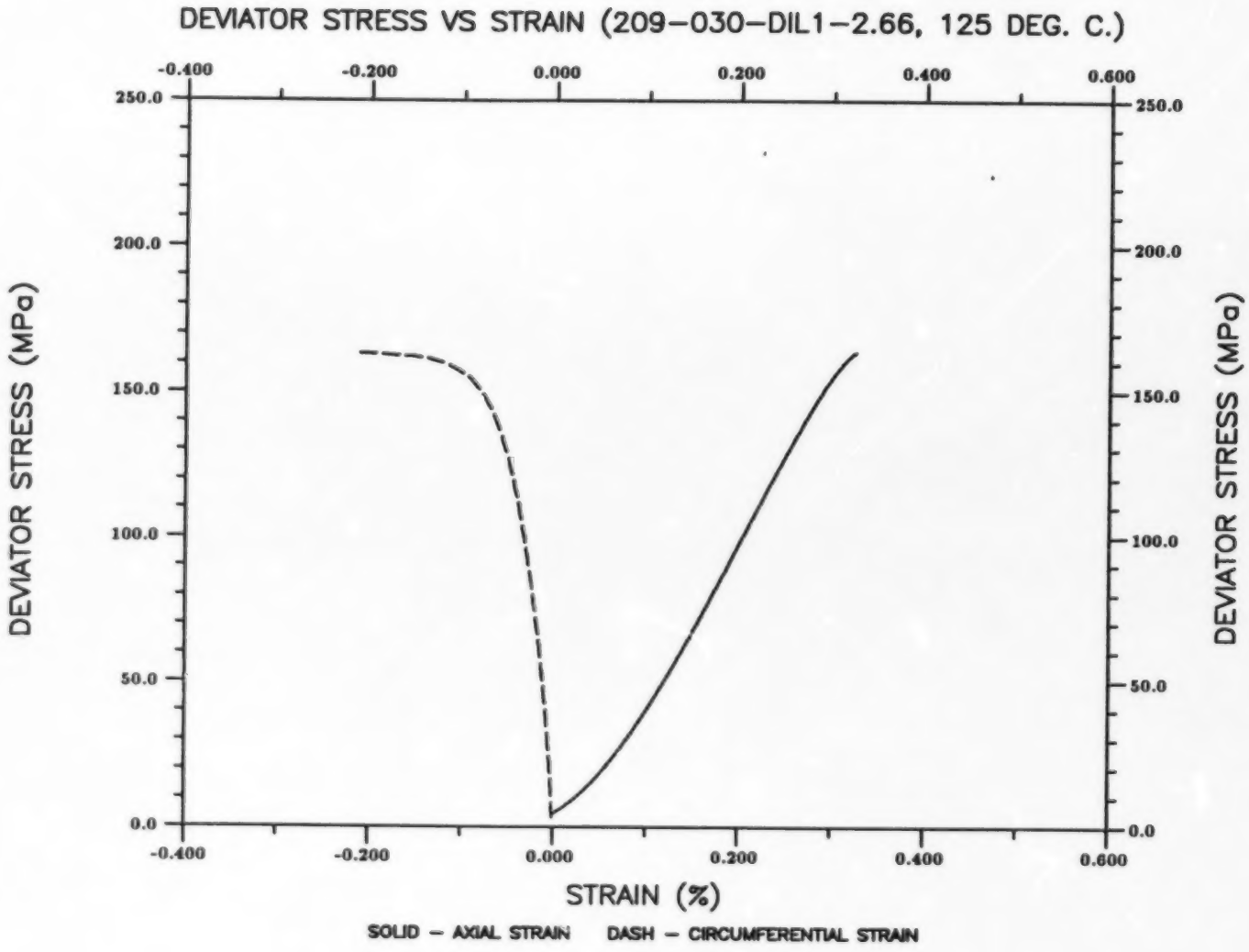

Figure B7. Stress-strain curves for Specimen 209-030-DIL1-2.66 tested at 125° C.

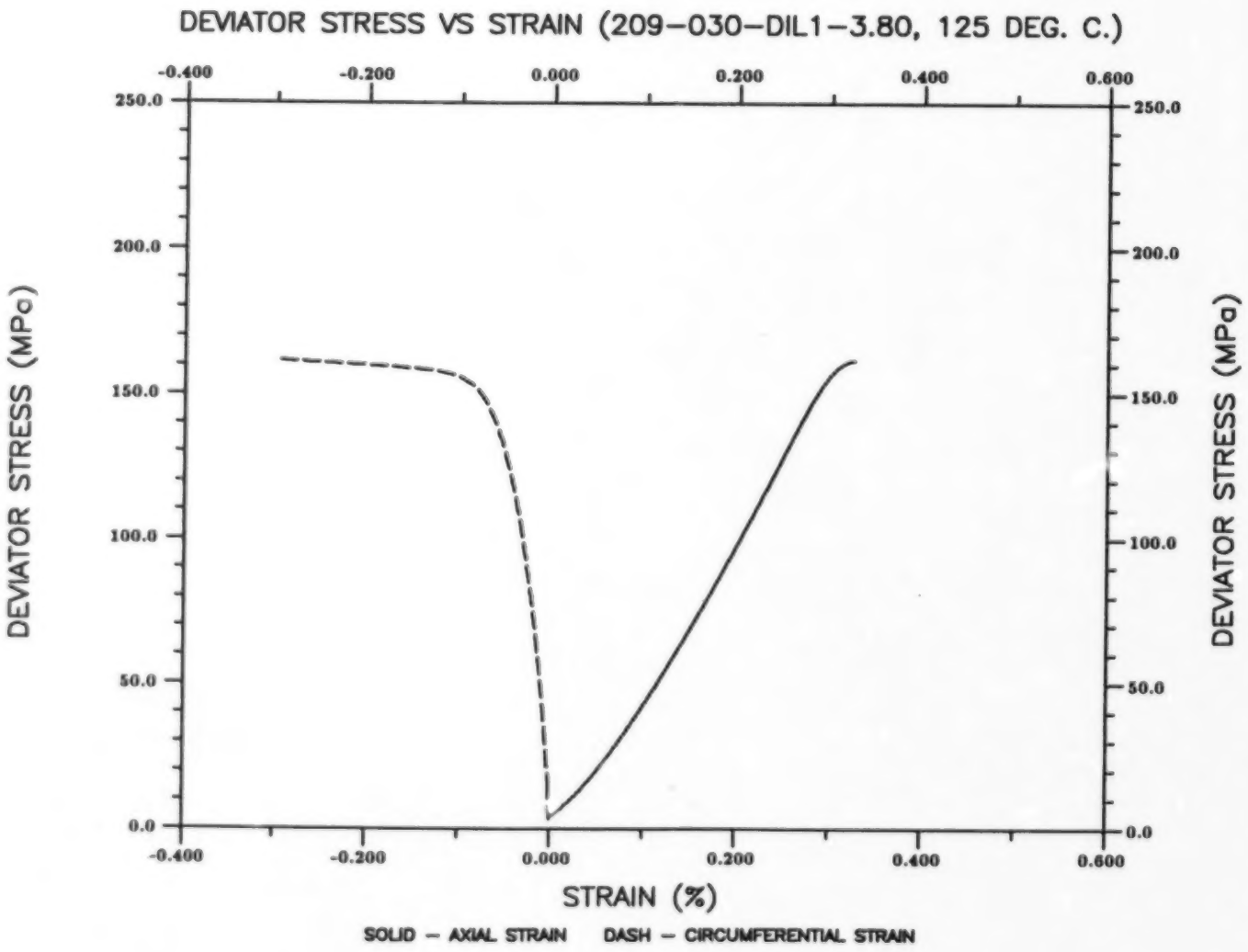

Figure B8. Stress-strain curves for Specimen 209-030-DIL1-3.80 tested at 125° C.